THE DETERMINATION OF THE SHAPE AND INERTIAL PROPERTIES OF AN ALL-FLEXIBLE PARAWING

By

Blair Bradley Gloss

Thesis submitted to the Graduate Faculty of the

Virginia Polytechnic Institute

in partial fulfillment for the degree of

MASTER OF SCIENCE

in

AEROSPACE ENGINEERING

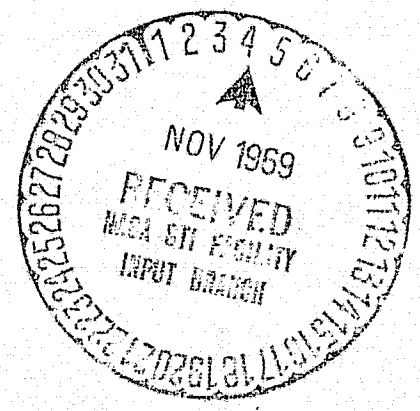

THE DETERMINATION OF THE SHAPE AND INERTIAL PROPERTIES OF AN ALL-FLEXIBLE PARAWING

by

Blair Bradley Gloss

Thesis submitted to the Graduate Faculty of the

Virginia Polytechnic Institute

in partial fulfillment for the degree of

MASTER OF SCIENCE

in

Aerospace Engineering

APPROVED:

Chairman, Dr. F. H. Lutze

Prof. W. D. Smith

Dr. F. R. DeJarnette

May 1969

Blacksburg, Virginia

THE DETERMINATION OF THE SHAPE AND INERTIAL PROPERTIES OF AN ALL-FLEXIBLE PARAWING

By

Blair Bradley Gloss

ABSTRACT

An investigation was conducted in the 17-foot test section of the 7- by 10-foot 300-MPH wind-tunnel at Langley Research Center to determine the shape of a 5-foot long, 45°-swept, single-keel, all-flexible parawing. A stereo-optic camera system was used to obtain shape data at lift-drag ratios of 2.429, 2.241, and 2.131. These data were used to calculate nondimensional moments of inertia, nondimensional products of inertia, and nondimensional center-of-gravity locations for the canopy alone and the suspension lines alone at lift-drag ratios of 2.429, 2.241, and 2.131. No estimates or calculations of moments of inertia were made for the apparent mass of the parawing system.

II. TABLE OF CONTENTS

III. ACKNOWLEDGEMENTS

The author wishes to thank the National Aeronautics and Space Administration, Langley Research Center, for the opportunity to write this thesis, for the aid and advice received during its preparation, and for typing this thesis.

He also wishes to thank Dr. Frederick H. Lutze of the Virginia Polytechnic Institute for his advice and assistance in preparing this thesis.

IV. LIST OF FIGURES AND TABLES

FIGURE PAGE

TABLE

V. INTRODUCTION

The National Aeronautics and Space Administration (NASA) at Langley Air Force Base has been working on flexible lifting devices for the past ten years. The first six years of work at NASA were focused on rigid-leading-edge and rigid-keel parawings, and the past four years have been spent primarily investigating all-flexible parawings which have been constructed in a variety of designs (see reference 1).

The advent of the decoupled lifting-entry vehicle, one which has been optimized for the hypersonic flight regime only, requires the need for some auxiliary devices to aid the vehicle in the supersonic and subsonic flight regimes. The all-flexible parawing is at present being considered by NASA as one such auxiliary device for the subsonic flight regime of this type of vehicle. More information about the all-flexible parawing, such as moments of inertia, shape data, and stability derivatives, to name a few, must be obtained in order to evaluate the all-flexible parawing as an auxiliary device.

After three years of research, no means of determining the shape of the all-flexible parawing had been found. Furthermore, moments of inertia of all-flexible parawings were previously determined by suspending the particular parawing of interest on a frame which weighed at least as much as the wing and swinging the entire system in the 60-foot vacuum sphere at NASA (see reference 2).

The purpose of this investigation was to obtain the shape of the 45°-swept, single-keel,all-flexible parawing using a photogrammetric process. From this shape data, the moments of inertia, the products of

inertia, and the center-of-gravity locations were calculated. The results were nondimensionalized so that they applied to any size 45°-swept, single-keel, all-flexible parawing with any weight material in the canopy and any weight suspension lines. The changes in moments of inertia, products of inertia, and center-of-gravity locations due to a change in lift-drag ratio were obtained.

VI. SYMBOLS

a	cross-sectional area of a suspension line, feet^2
b	distance between the stereo cameras, centimeters
c	focal length of the lens, centimeters
d	distance of a point to a coordinate plane, inches
A,B,C,DD	constants in the equation for a flat plane
I_{XX}	rolling moment of inertia, slugs-feet^2
I'_{XX}	transferred rolling moment of inertia, slugs-feet^2
I_{YY}	pitching moment of inertia, slugs-feet^2
I_{ZZ}	yawing moment of inertia, slugs-feet^2
I_{XY}	product of inertia, slugs-feet^2
I_{XZ}	product of inertia, slugs-feet^2
I_{YZ}	product of inertia, slugs-feet^2
LL	nondimensional suspension line lengths
L/D	lift-drag ratio
l_K	flat pattern keel length, inches
l_{KI}	inflated keel length, inches
l_s	inflated span, inches
m	mass of a small square of material in the canopy, slugs
M	total mass, slugs
n	total number of points read
p	difference between x'_{L_t} and x'_{R_t}, microns
XT	distance through which the glass plates must be translated in the x' direction, microns

YT	distance through which the glass plates must be translated in the y' direction, microns
X,Y,Z	body axis system with the origin at the confluence point
x,y,z	wind-tunnel axis system
x',y'	stereo-optic comparator axis system
x'',y''	glass plate axis system
x''',y''',z'''	stereo-optic camera's axis system
y'''_p	value of y''' when projected to the xz plane, inches
α, ϕ, θ	direction angles of a suspension line, degrees
Θ	transfer angle for the rolling moment of inertia, degrees
γ	transfer angle for the glass plates, degrees
ρ	density of the suspension lines, slugs/foot^3

Subscripts:

c	canopy
c.g.	center of gravity
L	suspension lines
L_t	left camera
R_t	right camera
1,2,3	ceiling reference point designations when associated with coordinates; coordinate plane designation when associated with A,B, and C

VII. MODEL

The flat pattern and suspension line lengths of the parawing that were used in this investigation are shown in figure 1 and table I, respectively. The line material was 130-pound test dacron. The wing was constructed of 1.1-ounce per square yard, acrylic-coated, ripstop white nylon, which is a low porosity material. Such material is required for maximum aerodynamic efficiency of the parawing. All seams were glued to prevent gathering of the material which always occurs with a sewn seam.

A reference system was printed on the canopy since, when reading the pictures taken by the stereo camera, it was necessary to be able to locate the same point in each picture. The reference system used is shown in figure 2. A 1/8-inch wide, black felt-tip pen was used to put the grid on the acrylic-coated side of the material which was on the bottom side of the wing.

VIII. TEST FACILITY AND EQUIPMENT

Wind-tunnel tests were conducted at atmospheric stagnation pressure in the 17-foot test section of the 7- by 10-foot 300-MPH wind-tunnel at Langley. Black cross marks, 1/2-inch wide, were painted on the test section ceiling every foot as shown in figure 3.

The wing was attached to the balance by means of a "T" bar, shown in figure 4. All the suspension lines were placed in the line clamp except for the three control lines which were tied on to the cross bar, shown in figures 3 and 5, to stabilize the model in pitch and roll.

The stereo camera system is shown set up in figures 3 and 5. This system consists of two camera units mounted rigidly 40 centimeters apart with parallel optical axes. Each camera has a focal length of 6.094 centimeters. Since these cameras had very high quality lenses, there was very little distortion on the pictures due to the lenses, and no correction for lens distortion was needed. The cameras were electrically operated so that both cameras' shutters were opened at the same instant. The pictures were taken on glass plates so that light could be projected through them for ease of reading.

Fiducial marks (reference marks) were put on the glass plates while they were still in the cameras by exposing each plate to four sources of radium in each camera for at least 1-1/2 minutes, but not more than 2 minutes.

IX. TEST CONDITIONS

The wind tunnel was operated at a dynamic pressure of 0.5 lbs/ft^2. Since the wing fluttered and vibrated least under this condition, all data were obtained at this dynamic pressure.

The lift-drag ratio was varied by shortening the eleventh keel line (see table I) while the support sting remained at zero angle of attack. Lift-drag ratio was used instead of angle of attack as the independent variable since there was not any accurate means for measuring the angle of attack of the wing while it was flying. Line lengths were measured immediately after each test.

The aerodynamic data were corrected for jet-boundary effects on flow angle (see reference 3), but not for blockage, since the blocking area of the wing was very small compared to the cross-sectional area of the wind tunnel.

X. SHAPE

A. Shape Data Reduction

Throughout this investigation, the all-flexible parawing was assumed to be symmetric about its keel; thus, the shape of only one lobe of the parawing was determined.

No special care was taken in aligning each picture (glass plate) on the stereo-optic comparator's tables since the plates were read individually and not in the usual stereo fashion. Figure 6 shows a typical setup on one of the comparator's tables. When reading these plates, it was necessary to locate the same point on each plate and determine the coordinates of that point on each plate with respect to the comparator's axis system. It was much simpler to read a point on one plate and then read that same point on the other plate, instead of the customary way of reading stereo pictures, which is to see the subject in stereo and locate the same point on each plate at the same time. The method of reading one plate at a time can only be done when the same point on each plate can be easily recognized separately of the other plate. All points that could be seen on both plates were read. The comparator automatically punched each set of coordinates of each point on IBM computer cards.

Both plates had to be mathematically rotated and translated so that the coordinate system of the comparator and the coordinate system of each glass plate exactly coincided. This necessitated operating on each set of coordinates by translating them XT in the x' direction and

YT in the y' direction, and rotating them through an angle of γ (see figure 6).

Figure 7 shows the geometry of transforming the two sets of two-dimensional coordinates into one set of three-dimensional coordinates. It can be easily seen from figure 7 that

$$x''' = \frac{b \cdot x'}{p}, \tag{1}$$

$$y''' = \frac{b \cdot c}{p}, \text{ and} \tag{2}$$

$$z''' = \frac{b \cdot y'}{p} \tag{3}$$

where b is the distance between the cameras (40 cm.) and c is the focal length of the lenses (6.094 cm). Since this three-dimensional coordinate system (x''',y''',z''') was not a particularly convenient system to work with, a method for transforming and rotating this system to the one shown in figure 8 was developed so that the angle of the cameras with respect to the vertical need not be known. This method is presented below.

Three of the painted cross marks on the ceiling (not in a straight line)were chosen as reference points, so that if straight lines were drawn joining them,a right triangle was formed that had one of its legs (not the hypotenuse) aligned with the flow in the wind tunnel. The numbered points in figure 8 were typical reference points. The coordinates of these points were determined in the x''',y''',z'''

coordinate system, and the equation of the ceiling plane (xy plane) was determined by solving the following simultaneous equations for A , B , and C where DD was chosen as unity (see references 4 and 5).

$$Ax_1''' + By_1''' + Cz_1''' + DD = 0 \quad (4)$$

$$Ax_2''' + By_2''' + Cz_2''' + DD = 0 \quad (5)$$

$$Ax_3''' + By_3''' + Cz_3''' + DD = 0 \quad (6)$$

To find the equation of the yz plane, the following set of simultaneous equations were solved for A_1 , B_1 , and C_1 .

$$A\,A_1 + B\,B_1 + C\,C_1 = 0 \quad (7)$$

$$A_1\,x_1''' + B_1\,y_1''' + C_1\,z_1''' + 1 = 0 \quad (8)$$

$$A_1\,x_3''' + B_1\,y_3''' + C_1\,z_3''' + 1 = 0 \quad (9)$$

To find the equation of the xz plane, the following set of simultaneous equations were solved for A_2 , B_2 , and C_2 .

$$A\,A_2 + B\,B_2 + C\,C_2 = 0 \quad (10)$$

$$A_2\,x_1''' + B_2\,y_1''' + C_2\,z_1''' + 1 = 0 \quad (11)$$

$$A_2\,x_2''' + B_2\,y_2''' + C_2\,z_2''' + 1 = 0 \quad (12)$$

Equations (7) and (10) satisfied the conditions that the xz and yz planes were perpendicular to the xy plane. The equations of the three coordinate planes were

$$A\,x''' + B\,y''' + C\,z''' + 1 = 0\,, \tag{13}$$

$$A_1\,x''' + B_1\,y''' + C_1\,z''' + 1 = 0\,, \text{and} \tag{14}$$

$$A_2\,x''' + B_2\,y''' + C_2\,z''' + 1 = 0\,. \tag{15}$$

To find the coordinates of a point in the coordinate system shown in figure 8, the distance of the point from each of the three coordinate planes were found by using the following equation:

$$d = \frac{\left| A\,x + B\,y + C\,z + DD \right|}{\sqrt{A^2 + B^2 + C^2}}\,. \tag{16}$$

Thus, the coordinate equations were

$$x = \frac{\left| A_1 x''' + B_1\,y''' + C_1\,z''' + 1 \right|}{\sqrt{A_1{}^2 + B_1{}^2 + C_1{}^2}}\,, \tag{17}$$

$$y = \frac{\left| A_2\,x''' + B_2\,y''' + C_2\,z''' + 1 \right|}{\sqrt{A_2{}^2 + B_2{}^2 + C_2{}^2}}\,, \text{ and} \tag{18}$$

$$z = \frac{\left| A\,x''' + B\,y''' + C\,z''' + 1 \right|}{\sqrt{A^2 + B^2 + C^2}}\,. \tag{19}$$

The reference points on the ceiling were carefully chosen so that the x and z coordinates were always positive. To determine the sign of the y coordinate of a point, the x''' and z''' coordinates of that point were put in equation (15) and then the equation was solved for y_p'''.

$$y_p''' = - \frac{\left(C_2 z''' + A_2 x''' + 1\right)}{B_2} \tag{20}$$

If y''' of the point was greater than y_p''', y was chosen as positive. A computer program was written that performed the above tasks for all points that were read.

Stereo plates were read for lift-drag ratios of 2.131, 2.241, and 2.429. Figure 26 shows that the inflated span increased with increasing lift-drag ratio, and the inflated keel length decreased with increasing lift-drag ratio. The aspect ratio, which was based on the projected area and the inflated span, remained constant with change in lift-drag ratio. The tunnel flight regime for this parawing was from a lift-drag ratio of 1.9 to 2.5. Since no accurate knowledge of the lift-drag ratio range in free flight had been obtained, the data in figure 26 were extrapolated in both directions to show trends.

B. Determination of Streamwise Sections

The streamwise sections of the wing were obtained by choosing a distance from the keel and finding coordinates with the proper value of y from the calculated data. If enough coordinates to define the shape of a section were not found, linear interpolations between points, which had y values close to the appropriate y value, were used to find the coordinates that were needed to describe the shape of that section. Very few interpolations were needed since there were approximately 3,300 points describing half the wing. Figures 9 to 25 show streamwise sections

for a parawing flying at an L/D of 2.241. The keel section could not be described because it could not be clearly seen on the glass plates. Thus, the first section shown is 0.4 of an inch from the keel. Streamwise sections were obtained every inch until at a spanwise position of 8.4 inches from the keel. After this spanwise location, the fabric was rather highly stretched, and there were fewer data points per unit area. The streamwise sections were then obtained only every two inches.

XI. ACCURACY OF THE SHAPE DATA

The only way to check the accuracy of the data was to compare the measured distances between the painted cross marks on the ceiling and the calculated distances between the same cross marks. Since the marks on the ceiling were 1/2-inch wide, it was impossible to locate the center of the marks while reading them on the comparator. Even with this inaccuracy, the calculated distances were off by only 3.33 percent or less (usually less).

Since the grid lines that were marked on the wing were about 1/8-inch wide, the accuracy of the wing shape data should be at least four times better than the accuracy of the calculated distances between the painted ceiling marks. Although there was no way to calculate the accuracy of the shape data, it is believed that the accuracy was approximately 0.8 percent.

XII. INERTIAL PROPERTIES

A. Determination of Inertial Properties

To obtain the shape used in calculating the moments of inertia, the plates were read again in a special manner. Again, the wing was assumed to be symmetrical about its keel. Instead of reading every point that could be seen, only the corners of the squares of the grid on the wing (shown in figure 2), the line attachment points on the canopy, and the confluence point of the lines were read on the stereo-optic comparator. Thus, all points that were read were centers of adjoining squares of material one square inch in area except at the boundaries (keel, trailing edge, leading edge, and nose), line attachment points on the canopy, and the confluence point. At the boundaries, the points that were read were not centers of squares, but they were assumed to be centers of odd-shaped pieces of material whose sizes were estimated when the point was read. The readings were reduced as described earlier.

The coordinate system shown in figure 8 was transferred to the coordinate system shown in figure 27, which is a body axis system with the origin at the confluence point of the lines. The wing was mathematically rotated about the X and Z axes so that the wing was not yawed or rolled.

Using the equations shown below (see reference 6), the moments of inertia and products of inertia were calculated for the canopy.

$$I_{XX} = \sum_{i=1}^{n} \left\{ 2 \left[\left(Y/l_K\right)^2 + \left(Z/l_K\right)^2 \right] m \right\}_i \tag{21}$$

$$I_{YY} = \sum_{i=1}^{n} \left\{ 2 \left[\left(X/l_K\right)^2 + \left(Z/l_K\right)^2 \right] m \right\}_i \tag{22}$$

$$I_{ZZ} = \sum_{i=1}^{n} \left\{ 2 \left[\left(X/l_K\right)^2 + \left(Y/l_K\right)^2 \right] m \right\}_i \tag{23}$$

$$I_{XZ} = - \sum_{i=1}^{n} \left[2 \left(X/l_K\right) \left(Z/l_K\right) m \right]_i \tag{24}$$

$$I_{XY} = 0.0 \tag{25}$$

$$I_{ZY} = 0.0 \tag{26}$$

In these equations, n was the total number of points read, and X , Y , and Z were the coordinates of the centers of the small pieces of material of the canopy. The terms that were summed were the moments and products of inertia of each small piece of material. The mass (m) was put to unity for all points that were centers of one square inch and put to the appropriate fractional value of unity for those points that were not centers of a square inch of material.

Since the coordinates of each end of all the lines were determined, the lengths of each line were calculated and nondimensionalized by dividing by l_K . Using the following equations, the moments of inertia and products of inertia for all the lines were calculated.

$$I_{XX} = \sum_{i=1}^{23} \left[\rho\, a \left(\sin^2 \phi + \sin^2 \theta \right) LL^3/3 \right]_i \tag{27}$$

$$I_{YY} = \sum_{i=1}^{23} \left[\rho\, a \left(\sin^2 \alpha + \sin^2 \theta \right) LL^3/3 \right]_i \tag{28}$$

$$I_{ZZ} = \sum_{i=1}^{23} \left[\rho\, a \left(\sin^2 \alpha + \sin^2 \phi \right) LL^3/3 \right]_i \tag{29}$$

$$I_{XZ} = -\sum_{i=1}^{23} \left[\rho\, a \sin \phi \sin \theta \left(LL^3/3 \right) \right]_i \tag{30}$$

$$I_{XY} = 0.0 \tag{31}$$

$$I_{YZ} = 0.0 \tag{32}$$

The terms in the brackets were the moments and products of inertia of an individual line. Figure 28 shows a typical line in the body axis system with direction angles ϕ, θ, and α. A value of unity was used for the product ρa in all calculations.

B. Determination of Center-of-Gravity Locations

The center of gravity of the canopy was calculated by using the following equations (see reference 6):

$$X_{c.g._c} = \sum_{i=1}^{n} \frac{\left[\left(X/l_K \right) m \right]_i}{M_c} \tag{33}$$

$$Y_{c.g._c} = \sum_{i=1}^{n} \frac{\left[\left(Y/l_K \right) m \right]_i}{M_c} \tag{34}$$

$$Z_{c.g._c} = \sum_{i=1}^{n} \frac{\left[\left(Z/l_K\right) m\right]_i}{M_c} \tag{35}$$

Where X, Y, and Z were the coordinates of the centers of each small piece of material, m was handled as described earlier, and M_c was the sum of all the m's.

The center of gravity of the lines was calculated by using the following equations:

$$X_{c.g._L} = \sum_{i=1}^{23} \frac{\left[\left(X/l_K\right)\left(\rho\ a\right) LL\right]_i}{M_L} \tag{36}$$

$$Y_{c.g._L} = \sum_{i=1}^{23} \frac{\left[\left(Y/l_K\right)\left(\rho\ a\right) LL\right]_i}{M_L} \tag{37}$$

$$Z_{c.g._L} = \sum_{i=1}^{23} \frac{\left[\left(Z/l_K\right)\left(\rho\ a\right) LL\right]_i}{M_L} \tag{38}$$

where X, Y, and Z were the coordinates of the centers of gravity of each line. Since the product $\rho\ a$ is unity, M_L is the sum of the LL's.

Table II shows the results of the inertial and center-of-gravity calculations for lift-drag ratios of 2.131, 2.241, and 2.429.

XIII. RESULTS AND DISCUSSION

A. The Parawing Shape

Since, when the plates were read, no attempt was made to read small wrinkles in the canopy, the streamwise sections were fairly smooth. The deep wrinkles in the sections shown in figures 17 and 22 were due to canopy line attachments which were close to these deep wrinkles. The section shown in figure 25 occurred because the tips (last lines on the leading edges) doubled back under the canopy. A close examination of figure 3 will show that these sections were possible and were, in fact, expected.

Figure 26 shows that, while lift-drag ratios increased from 2.131 to 2.439, the inflated span increased 3.6 percent, the inflated keel length decreased 3.0 percent, and the aspect ratio, which was based on the projected area and inflated span, remained constant.

As can be seen from figures 9 to 25, this parawing has extremely large amounts of dihedral, twist, and camber. As a measure of twist, the streamwise sections vary in angle of attack from 11.5° to 39°.

B. Inertial Properties

With the lift-drag ratio increased from 2.131 to 2.429, the following changes in the inertial properties of the canopy were noted: I_{XX} increased 4.4 percent, I_{YY} increased 0.5 percent, I_{ZZ} decreased 17.8 percent, and I_{XZ} decreased 8.6 percent. With the same change in lift-drag ratio, the following changes in the inertial properties of the lines were noted: I_{XX} increased 6.0 percent, I_{YY} increased 1.9 percent, I_{ZZ} decreased 18.5 percent, and I_{XZ} decreased 9.8 percent. Figure 29

shows that the wing essentially rotated around its confluence point with change in lift-drag ratio, and figure 26 shows that the canopy shape did change somewhat with change in lift-drag ratio. The above changes in I_{XX} , I_{ZZ} , and I_{XZ} were mainly due to the wing's rotation about its confluence point. The small changes in I_{YY} were caused by the change in canopy shape.

C. Comparison of Inertial Results With Another Investigation

The pitching and rolling moments of inertia and the center of gravity for a 24-foot, 45°-swept, single-keel, all-flexible parawing were measured by swinging this wing in a vacuum about its confluence point while the canopy was held in its approximate shape by a light-weight frame (see reference 2). The weight of the lines of this wing was 4.6 grams per foot of length, and the average weight of the material of the canopy was 5.07 ounces per yard.

Since this wing was suspended and not flying, the wing angle of attack was off by 26.5° from its flying angle of attack. Thus, in order to compute the measured and calculated rolling moment of inertia, the following equation was used to transfer the calculated rolling moment of inertia through 26.5° (see reference 6):

$$I'_{XX} = I_{XX} \cos^2 \theta + I_{ZZ} \sin^2 \theta - 2 I_{XZ} \sin \theta \cos \theta . \qquad (39)$$

The values of I_{XX} , I_{ZZ} , and I_{XZ} that were used in equation (39) were 392.1 slugs-ft^2, 119.5 slugs-ft^2, and -185.2 slugs-ft^2, respectively.

The calculated value of I'_{XX} was 486.1 slugs-ft^2, while the measured rolling moment of inertia was 502.5 slugs-ft^2. The calculated pitching moment of inertia was 478.4 slugs-ft^2, while the measured value was 501.6 slugs-ft^2.

The Appendix shows the method used in calculating the moments and products of inertia from the nondimensional values in Table II.

Figure 30 shows a comparison of the calculated and measured center of gravity of the 24-foot wing in question.

XIV. CONCLUDING REMARKS

An investigation to determine the shape and inertial properties of an all-flexible parawing indicated the following conclusions:

1. Photogrammetric techniques can be used to obtain accurate shape and inertia data of an all-flexible parawing.

2. Since this parawing had such high camber, twist, and dihedral, a three-dimensional, aerodynamic analysis, such as the Weissinger-L method, would be extremely difficult.

3. The inertial properties and shape of this parawing cannot be assumed constant with change in lift-drag ratio.

XV. REFERENCES

1. Naeseth, Rodger L.; and Fournier, Paul G.: Low-Speed Wind-Tunnel Investigation of Tension-Structure Parawings. NASA TN D-3940, 1967.

2. Sumners, Dan O.: Inertia Tests of a 24-Foot Single-Keel Parawing NASA CR-66744, November 1968.

3. Gillis, Clarence L.; Polhamus, Edward C.; and Gray, Joseph L.: Charts for Determining Jet-Boundary Corrections for Complete Models in 7- by 10-Foot Closed Rectangular Wind Tunnels. NACA WRL-123, 1945.

4. McCoy, Neal H.; and Johnson, Richard E.: Analytic Geometry. Holt, Rinehart, and Winston, New York, 1960.

5. Wilson, W. A.; and Tracey, J. I.: Analytic Geometry. D. C. Heath and Company, Boston, 1949.

6. Pletta, Dan H.; and Frederick, Daniel: Engineering Mechanics Statics and Dynamics. The Ronald Press Company, New York, 1964.

XVI. VITA

The author was born [redacted] in [redacted]. He graduated from Washington Irving High School in Clarksburg, West Virginia, in 1961. In 1966, he received a Bachelor of Science degree in Aerospace Engineering from the Virginia Polytechnic Institute. Since graduation, he has been employed by the National Aeronautics and Space Administration at Langley Research Center, Hampton, Virginia.

XVII. APPENDIX

The procedure for calculating the pitching moment of inertia for the canopy alone of a 24-foot parawing at a L/D of 2.131 is as follows:

$$I_{YY_c} = \left(4118.493\right)\left(24\ \text{ft}\right)^2\left(\frac{24\ \text{ft}}{5\ \text{ft}}\right)^2 \left(\frac{5.07\ \text{oz/yd}^2}{16\ \text{oz/lb} \times 32.2\ \text{ft/sec}^2 \times 9\ \text{ft}^2\text{/yd} \times 144\ \text{in}^2\text{/ft}}\right)$$

$$I_{YY_c} = 415\ \text{slugs-ft}^2$$

The third term scales the one-square inch pieces of material that were used to calculate the moments of inertia of the 5-foot wing to the appropriate size square for a 24-foot wing. The fourth term is the calculation of the mass of one-square inch of material.

The procedure for calculating the pitching moment of inertia for the lines of a 24-foot parawing at a L/D of 2.131 is as follows:

$$I_{YY_L} = \left(14.54\right)\left(24\ \text{ft}\right)^3\left(\frac{4.6\ \text{grams/ft}}{453\ \text{grams/lb} \times 32.2\ \text{ft/sec}^2}\right) = 63.4\ \text{slugs-ft}^2$$

The total pitching moment of inertia is 478.4 slugs-ft^2.

TABLE I

LINE LENGTHS (INCHES)

Line No.	L/D	Keel	Right Leading Edge	Left Leading Edge
1		81	82	81-7/8
2		81-5/8	78-1/4	78-7/8
3		81-1/8	75-1/2	75-5/8
4		80-3/8	72-1/8	72-7/8
5		79-3/8	69-15/16	68-5/8
6		78-3/8	59-5/8	59
7		77-1/2		
8		76-1/8		
9		74-1/2		
10		72-5/16		
11	2.429	65-1/2		
11	2.241	64-1/2		
11	2.131	64		

TABLE II

INERTIAL AND CENTER-OF-GRAVITY DATA

Nondimensional Inertial Properties of the Canopy

L/D	I_{XX}	I_{YY}	I_{ZZ}	I_{XZ}	I_{ZY}	I_{XY}
2.429	3504.294	4113.679	875.341	-1484.800	0	0
2.241	3364.880	4137.219	1040.183	-1621.751	0	0
2.131	3349.387	4118.493	1064.590	-1624.178	0	0

Nondimensional Inertial Properties of the Lines

L/D	I_{XX}	I_{YY}	I_{ZZ}	I_{XZ}	I_{ZY}	I_{XY}
2.429	13.276	14.812	2.282	-4.465	0	0
2.241	12.609	14.549	2.728	-4.881	0	0
2.131	12.523	14.540	2.799	-4.952	0	0

Center-of-Gravity Coordinates for the Lines and Canopy in Percent, l_K

L/D	$X_{c.g._L}$	$Y_{c.g._L}$	$Z_{c.g._L}$	$X_{c.g._c}$	$Y_{c.g._c}$	$Z_{c.g._c}$
2.429	0.210	0	0.575	0.529	0	1.164
2.241	0.237	0	0.560	0.586	0	1.133
2.131	0.241	0	0.550	0.592	0	1.131

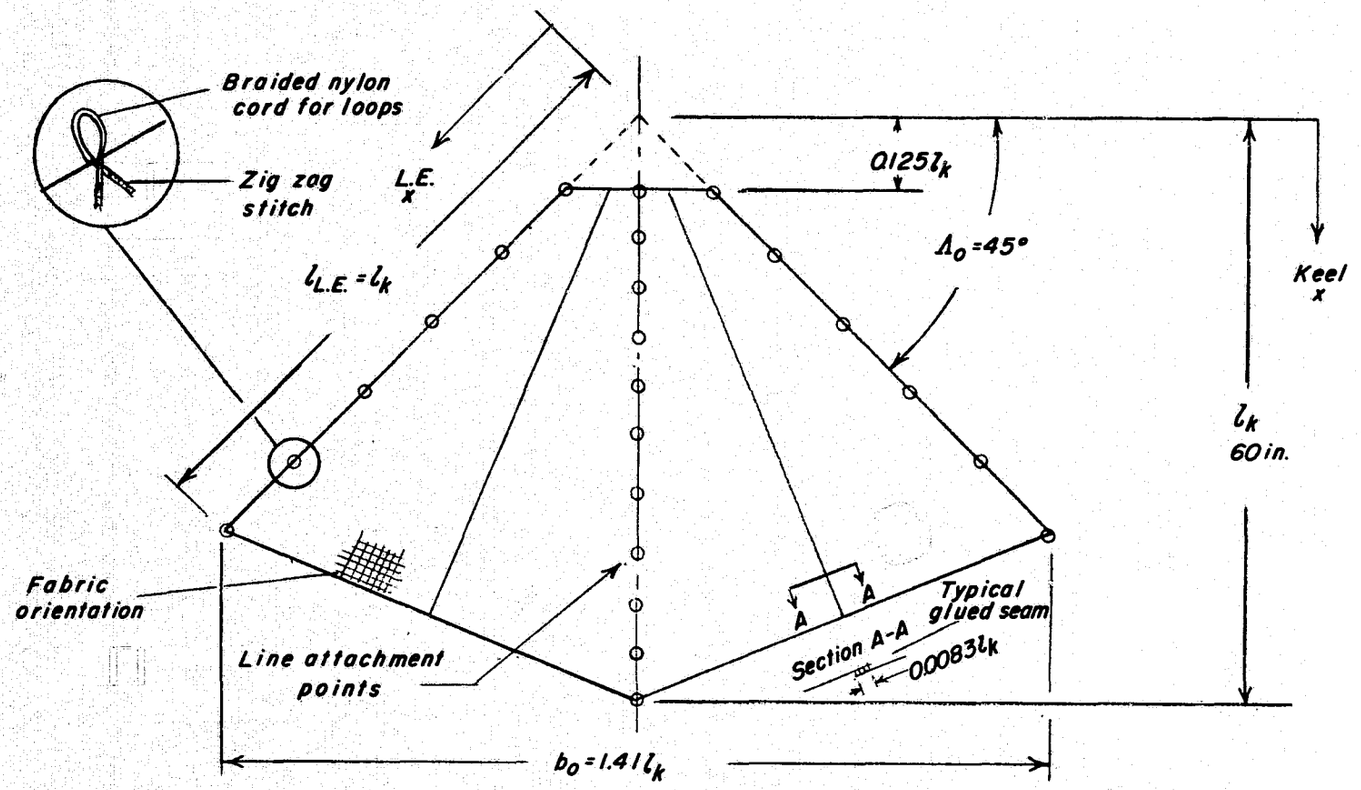

Line attachment locations

	x/l_k Keel		Leading edge
1	.125	1	.177
2	.208	2	.333
3	.292	3	.500
4	.375	4	.667
5	.459	5	.833
6	.542	6	1.000
7	.645		
8	.750		
9	.833		
10	.917		
11	1.000		

Figure 1. - Construction details of the parawing.

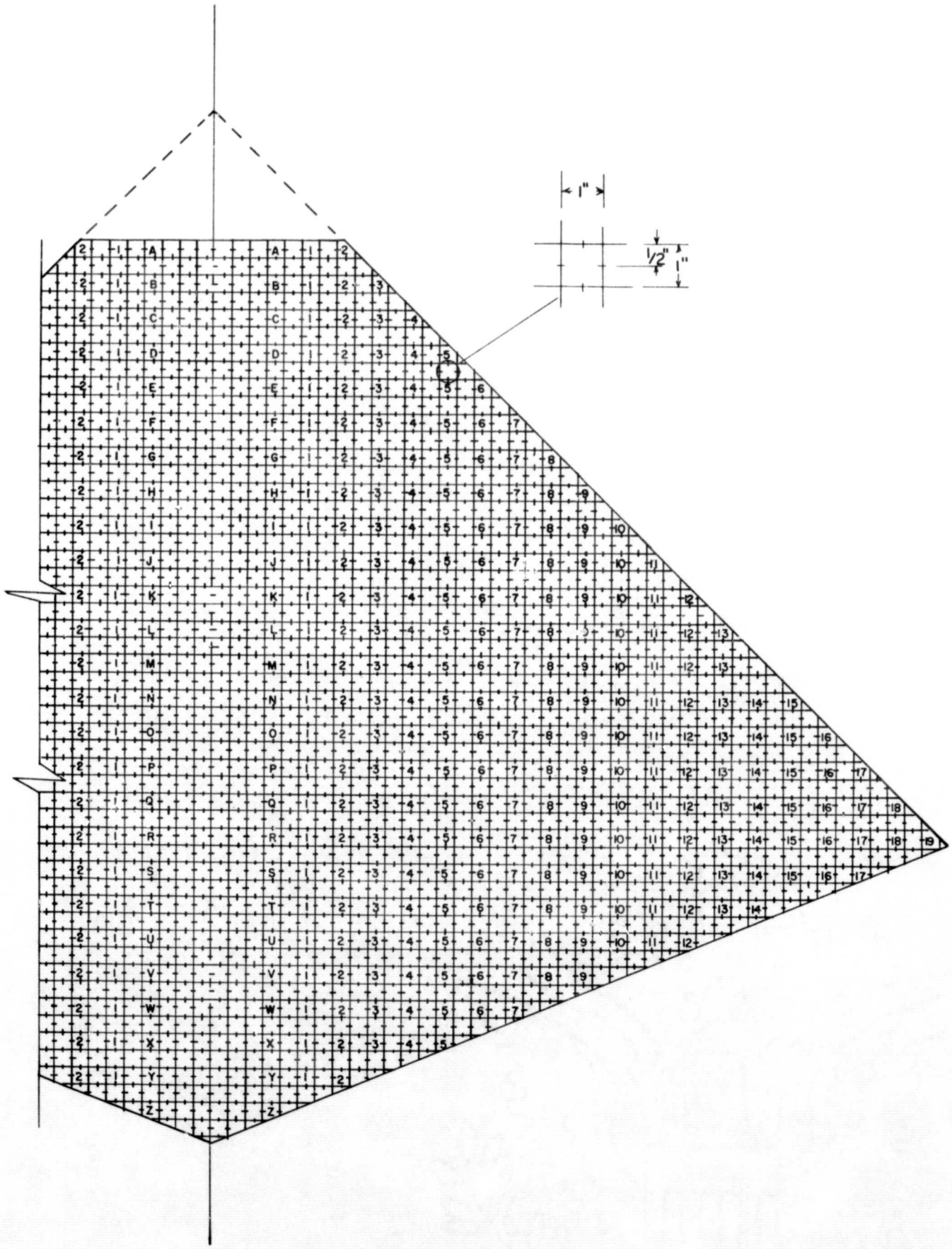

Figure 2. - The canopy reference system.

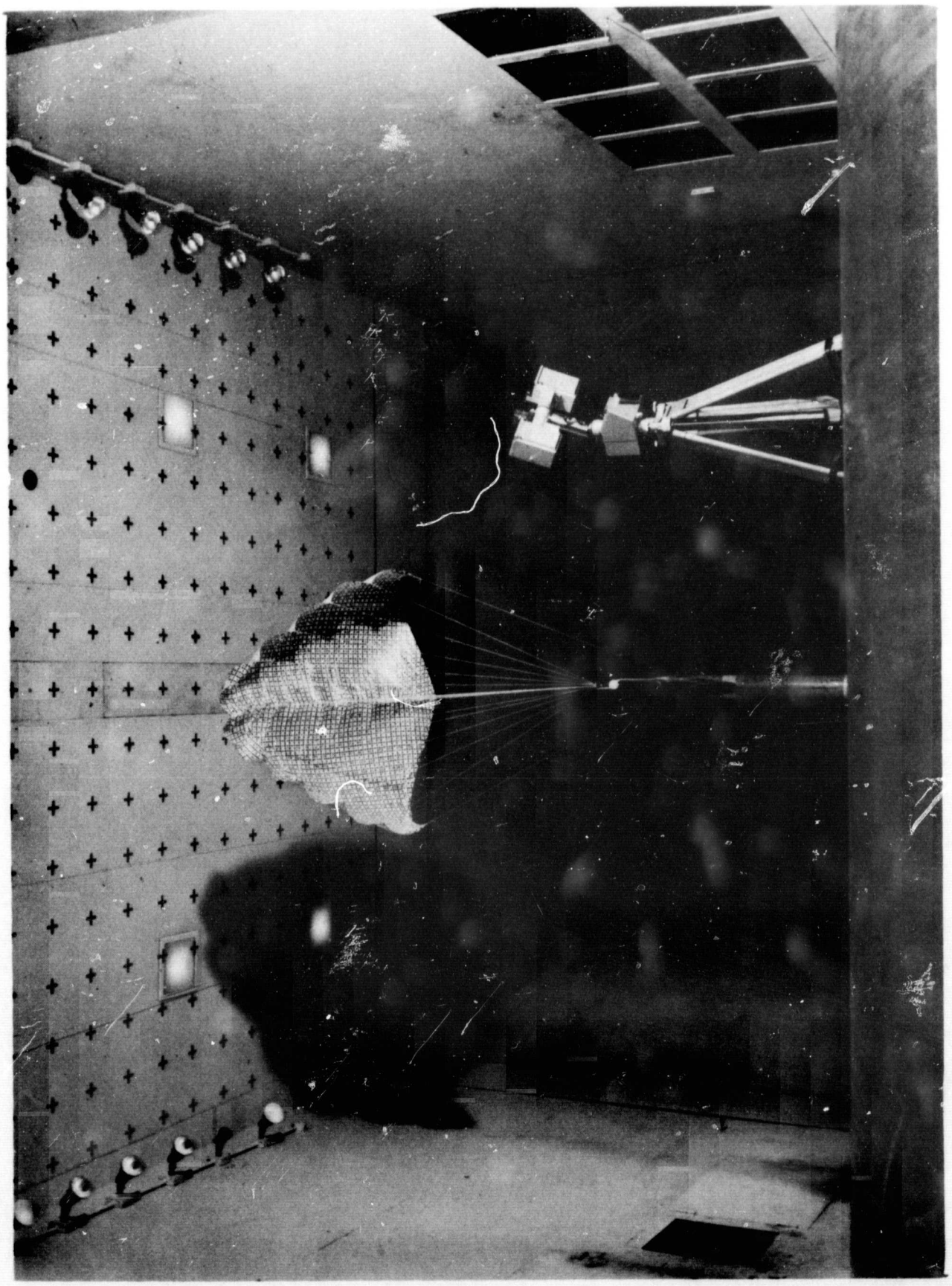

Figure 3. - Front view of the test section setup.

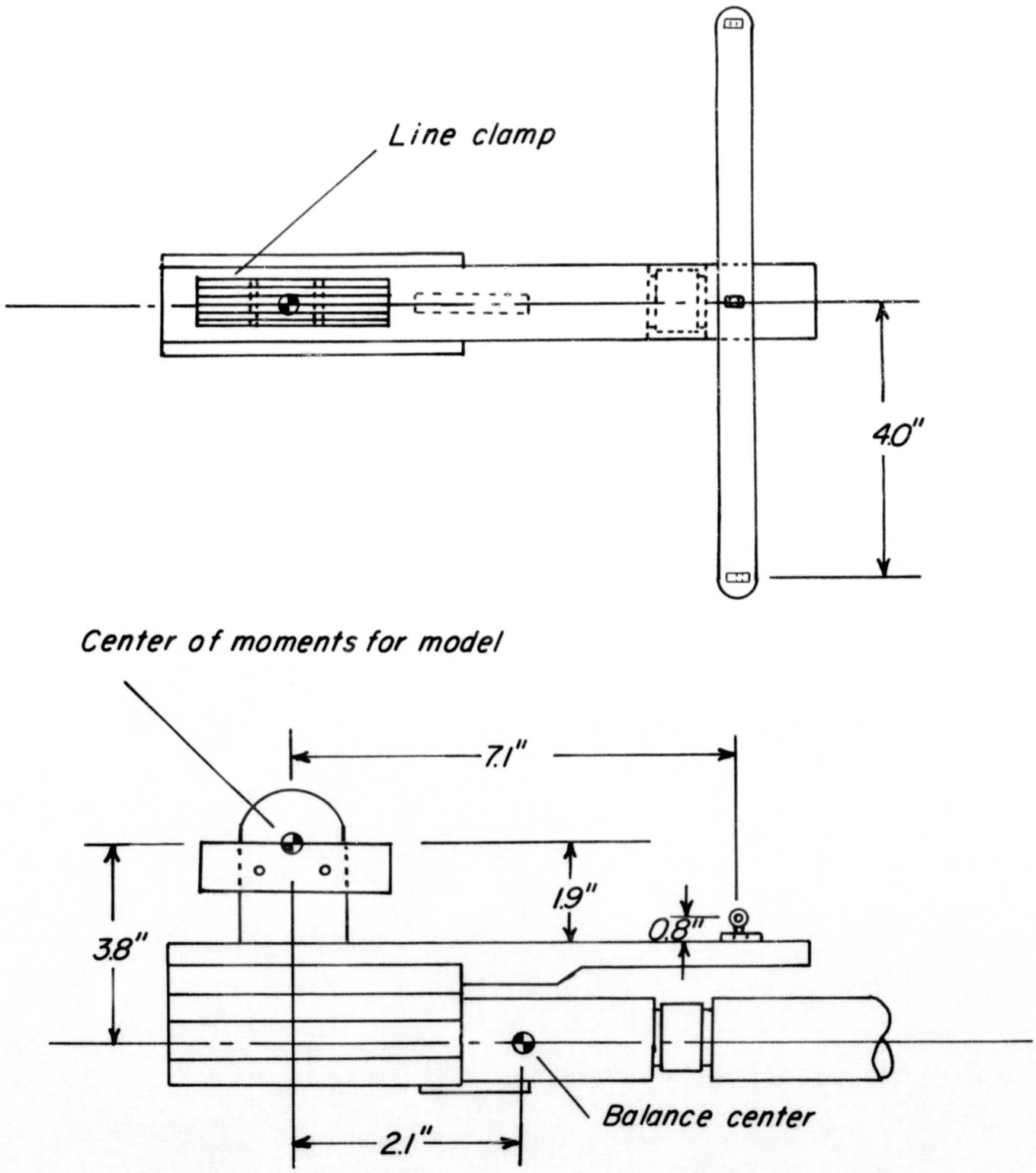

Figure 4. - "T" bar used in wind-tunnel tests.

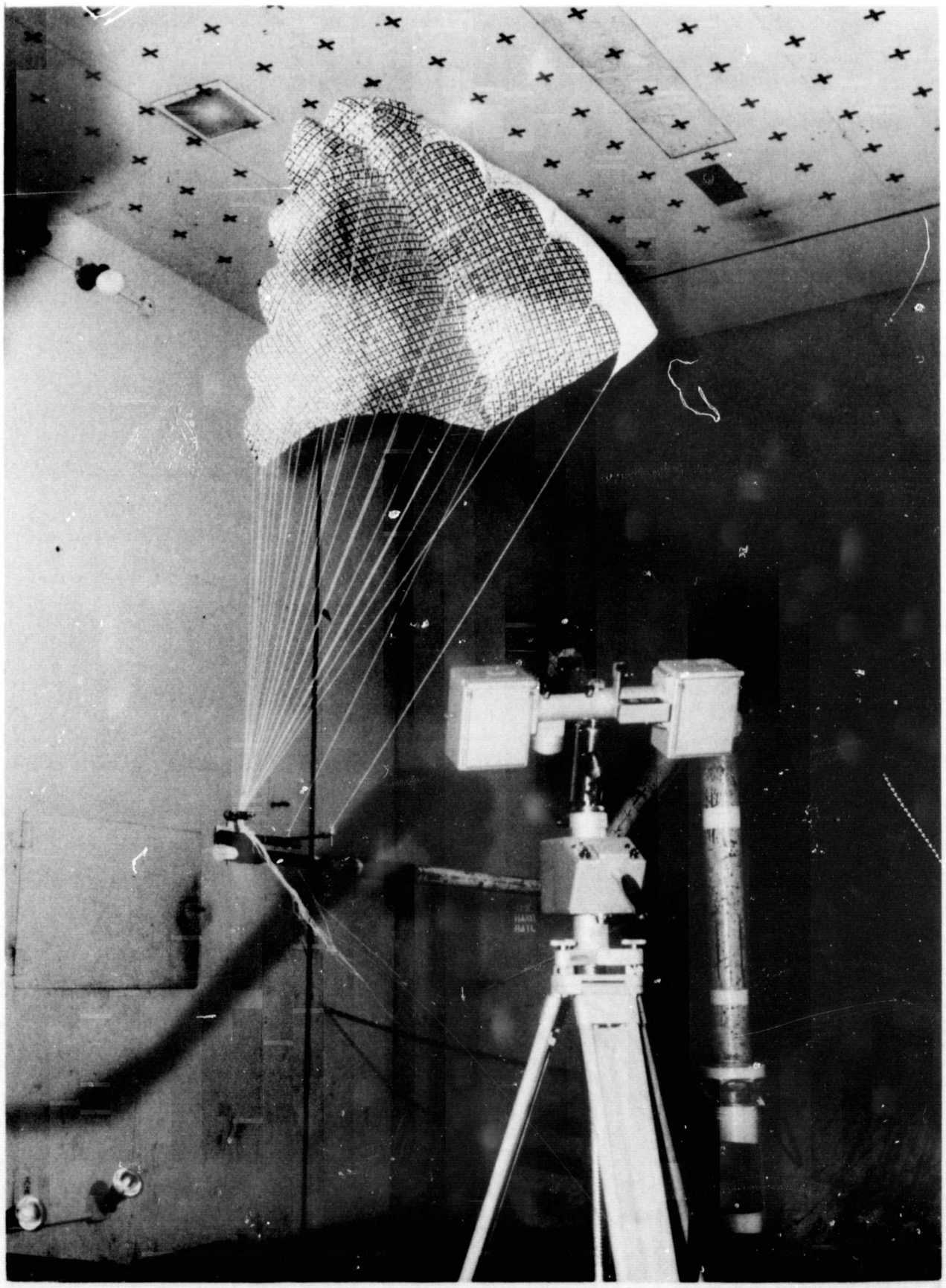

Figure 5. - Side view of the test section setup.

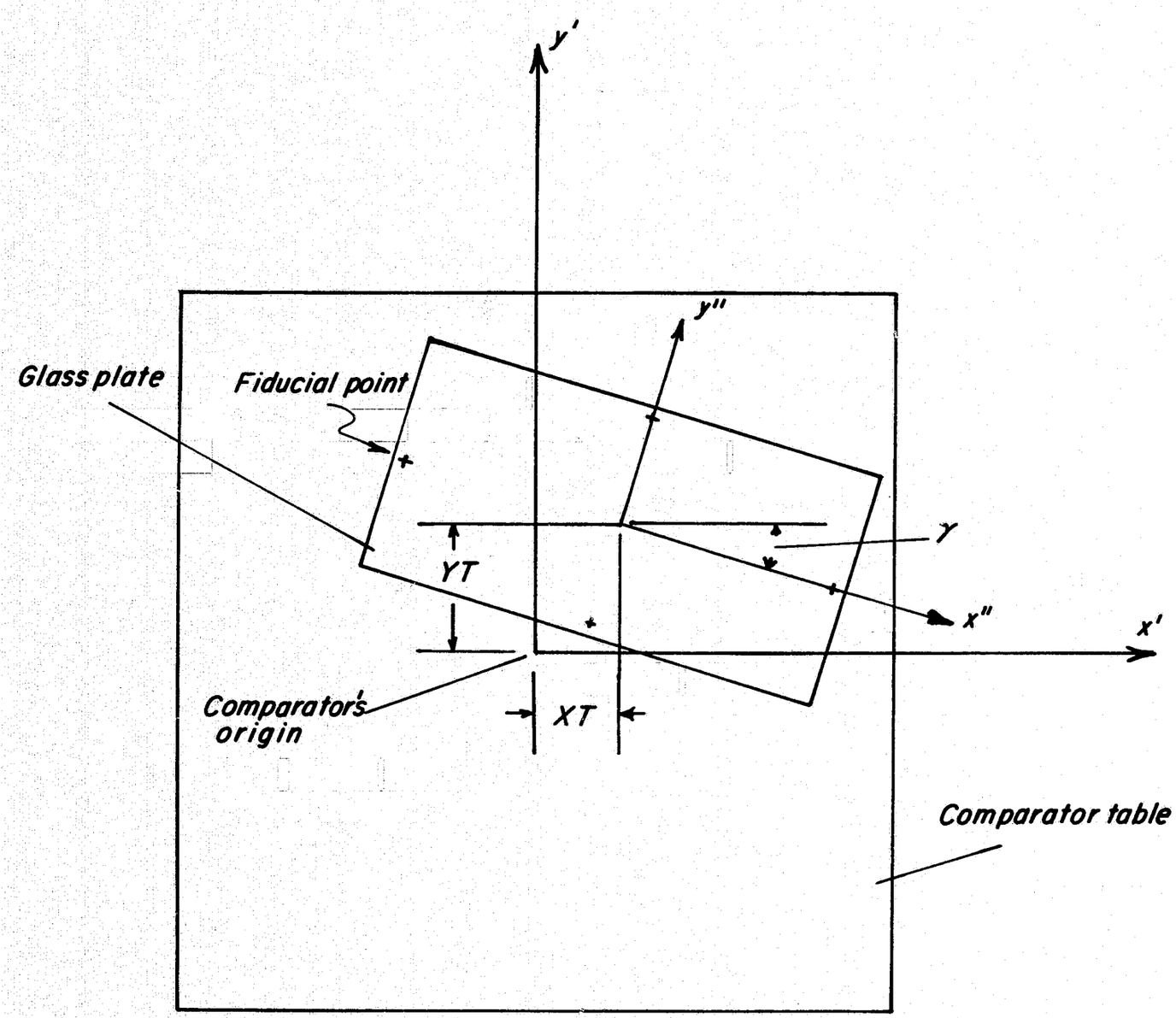

Figure 6. - Typical comparator table setup.

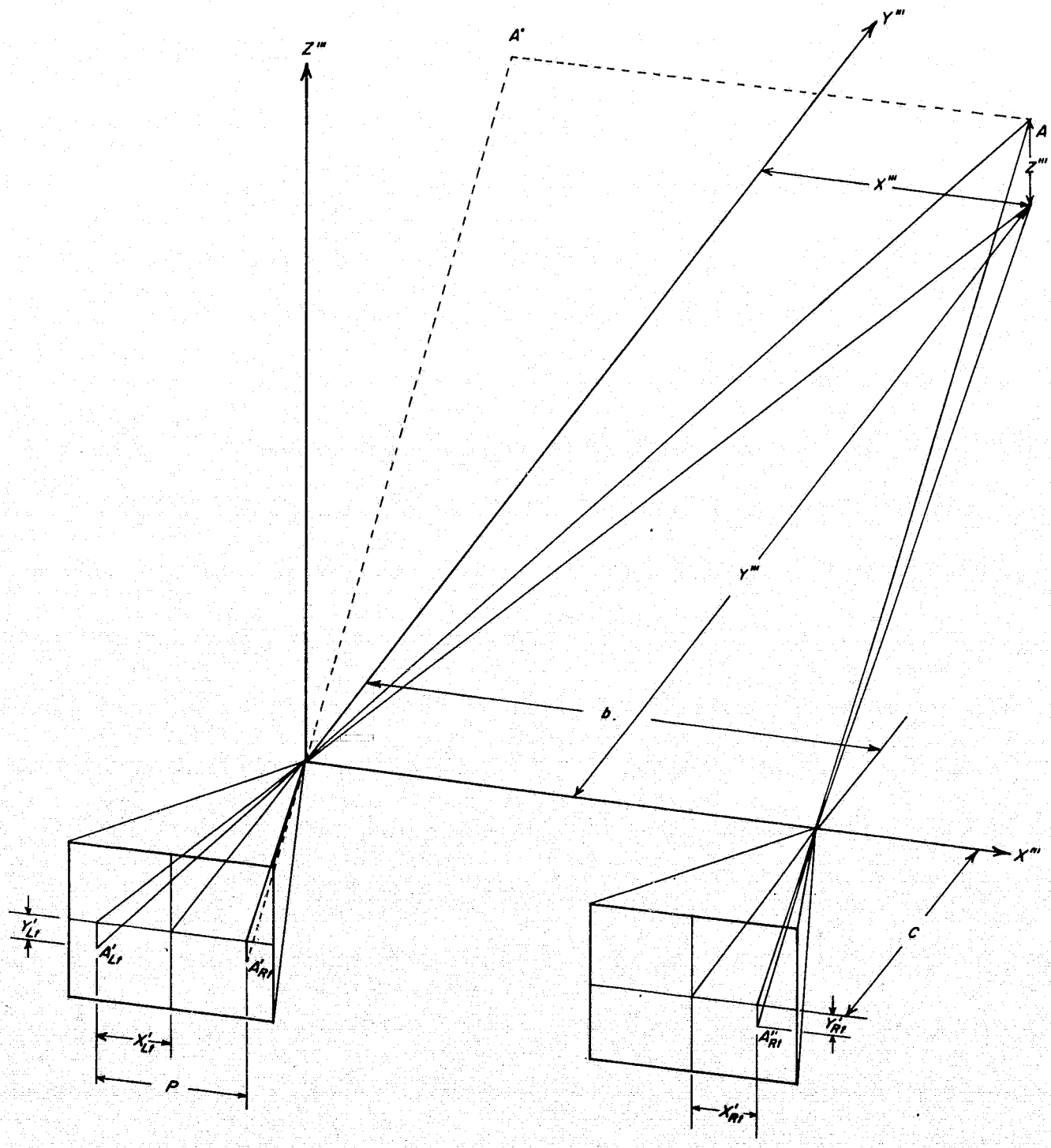

Figure 7. - The geometry of obtaining the three-dimensional coordinates.

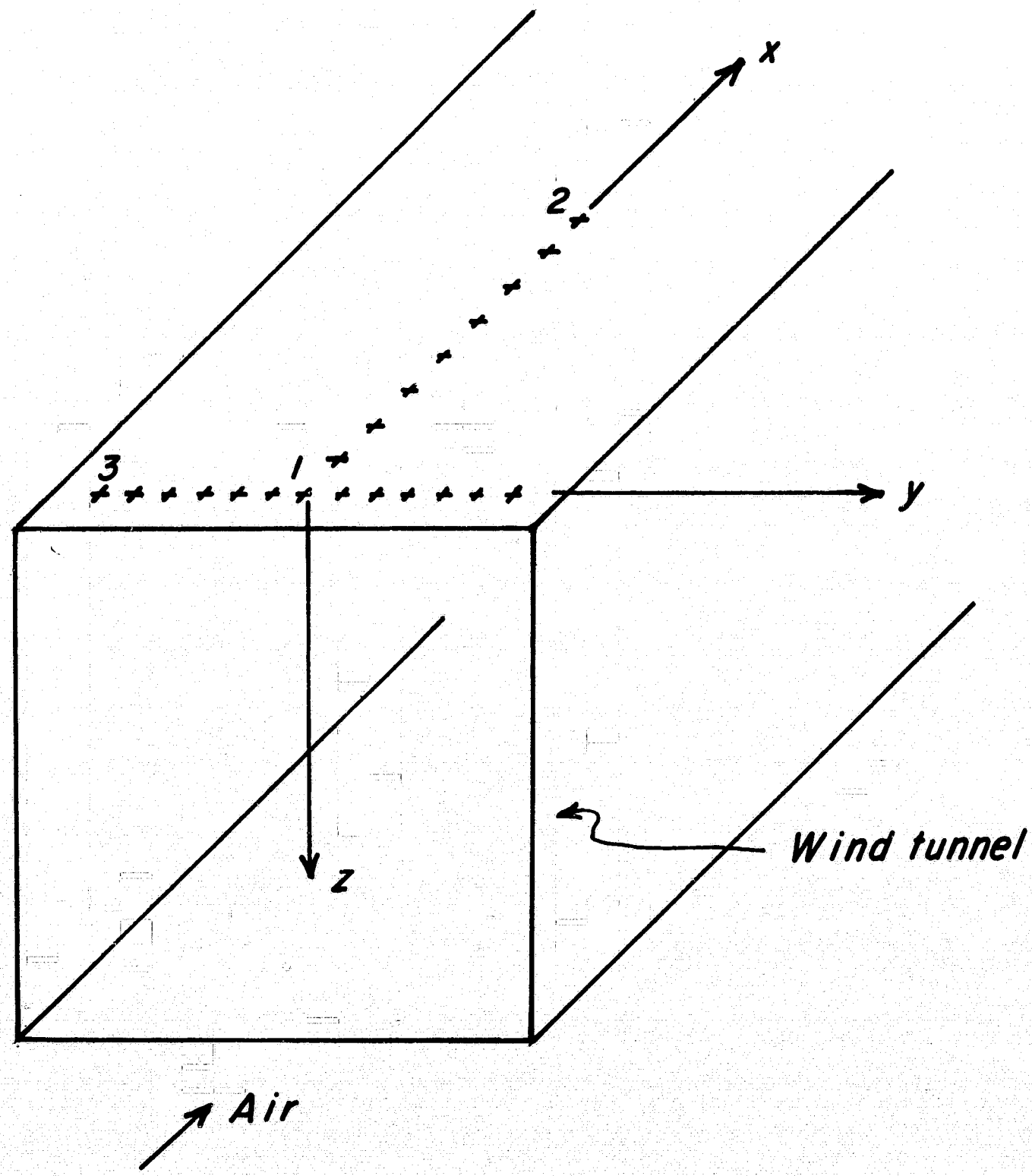

Figure 8. - Wind-tunnel-oriented coordinate system.

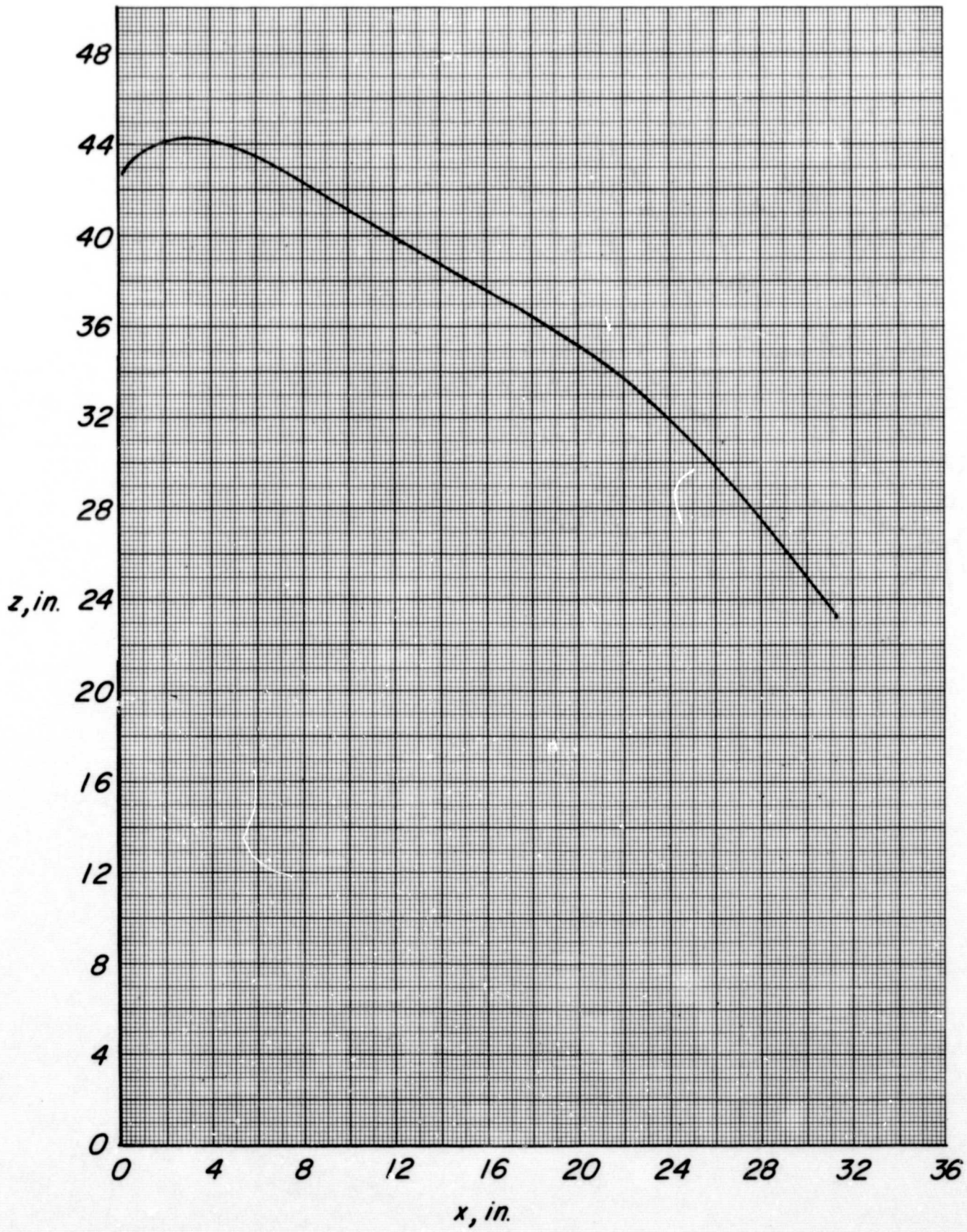

Figure 9. - Streamwise section 0.4 inches from the keel.

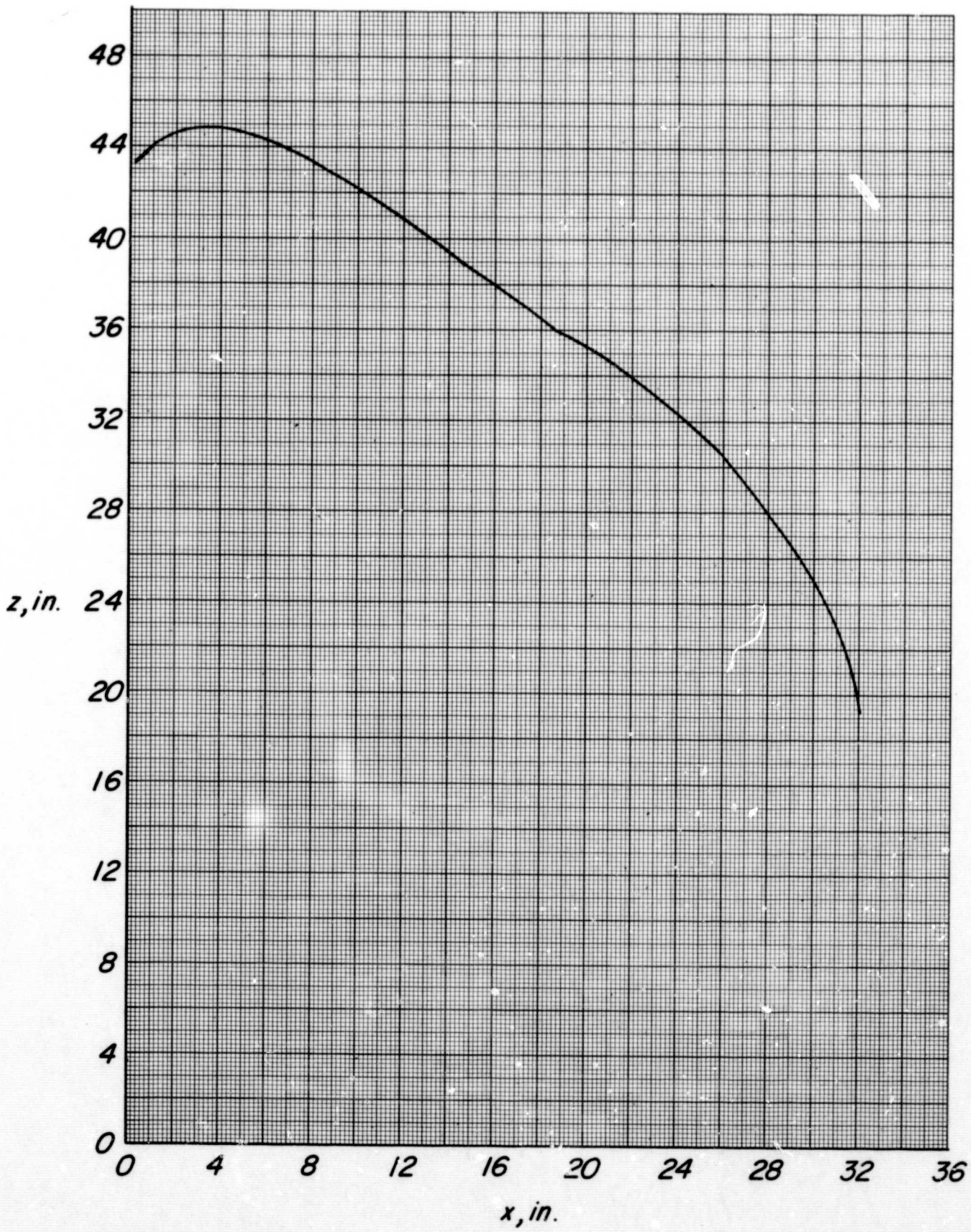

Figure 10. - Streamwise section 1.4 inches from the keel.

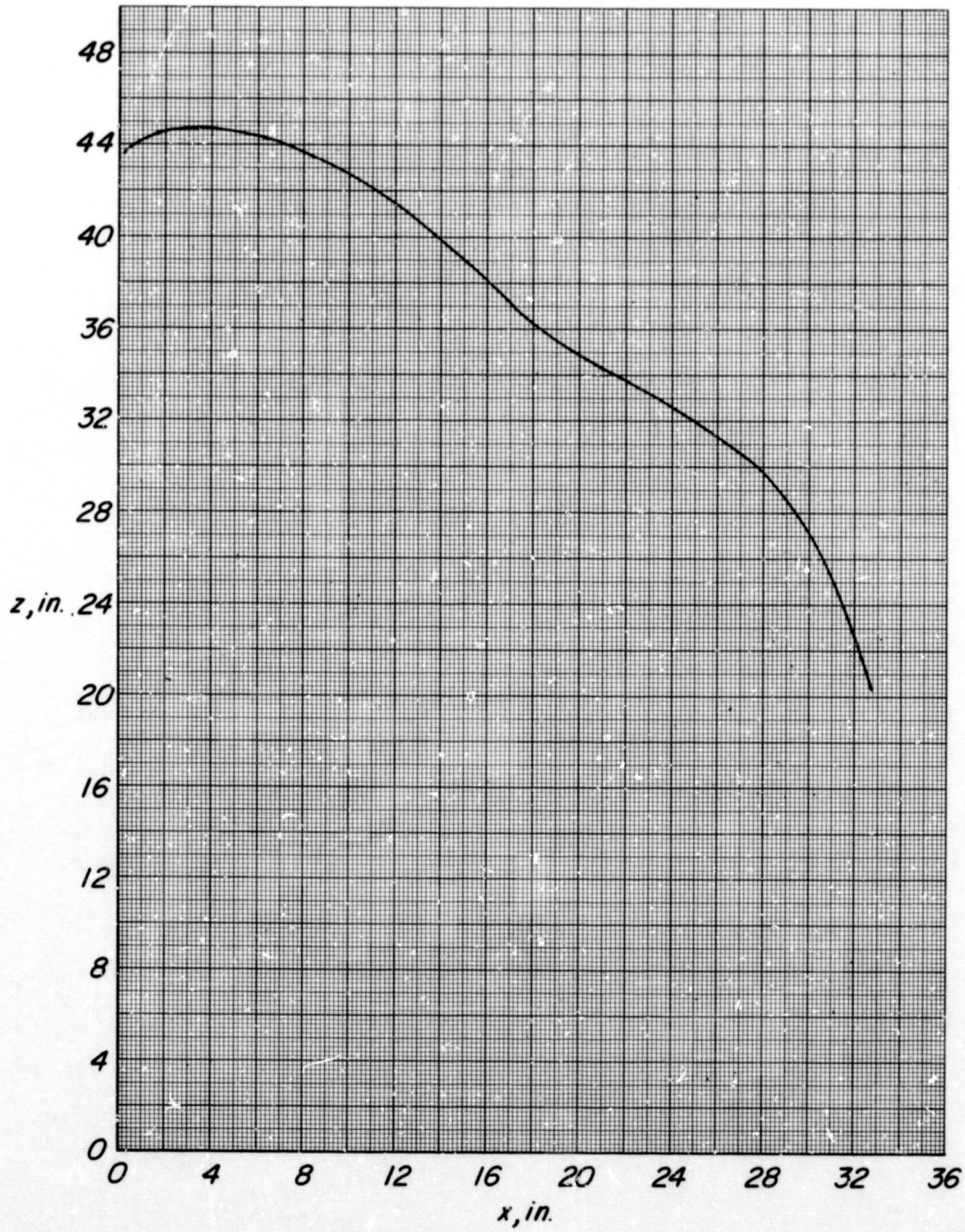

Figure 11. - Streamwise section 2.4 inches from the keel.

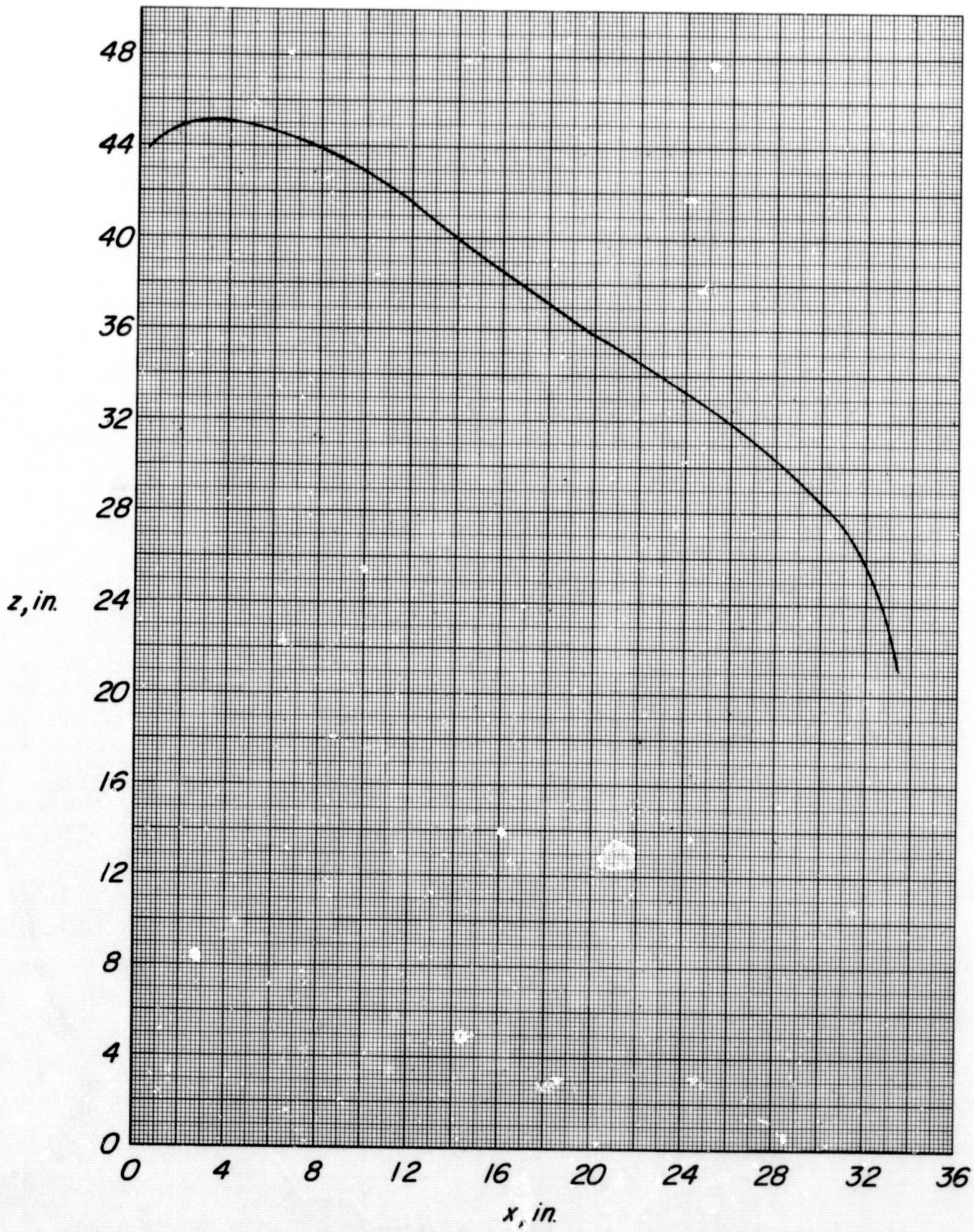

Figure 12. - Streamwise section 3.4 inches from the keel.

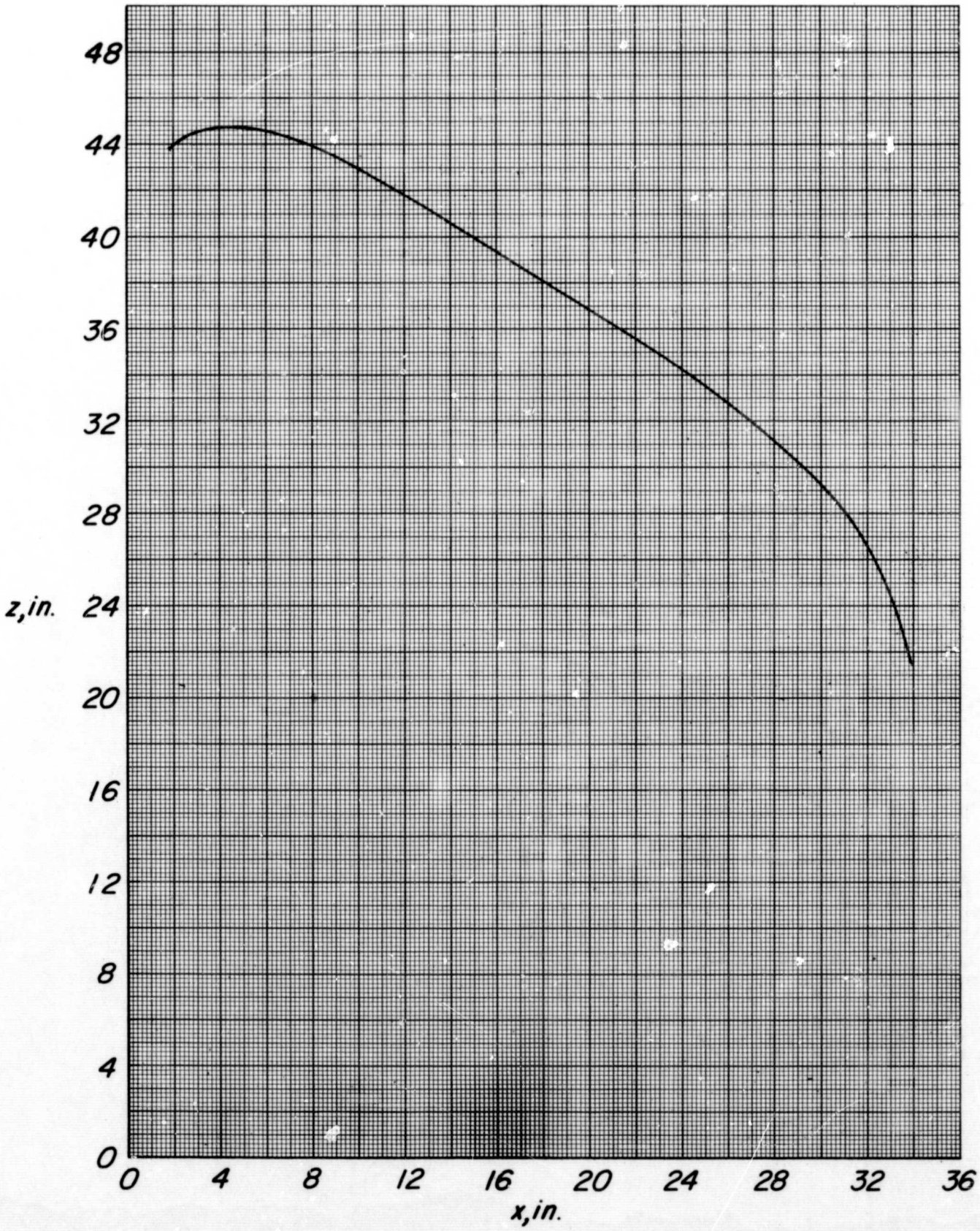

Figure 13. - Streamwise section 4.4 inches from the keel.

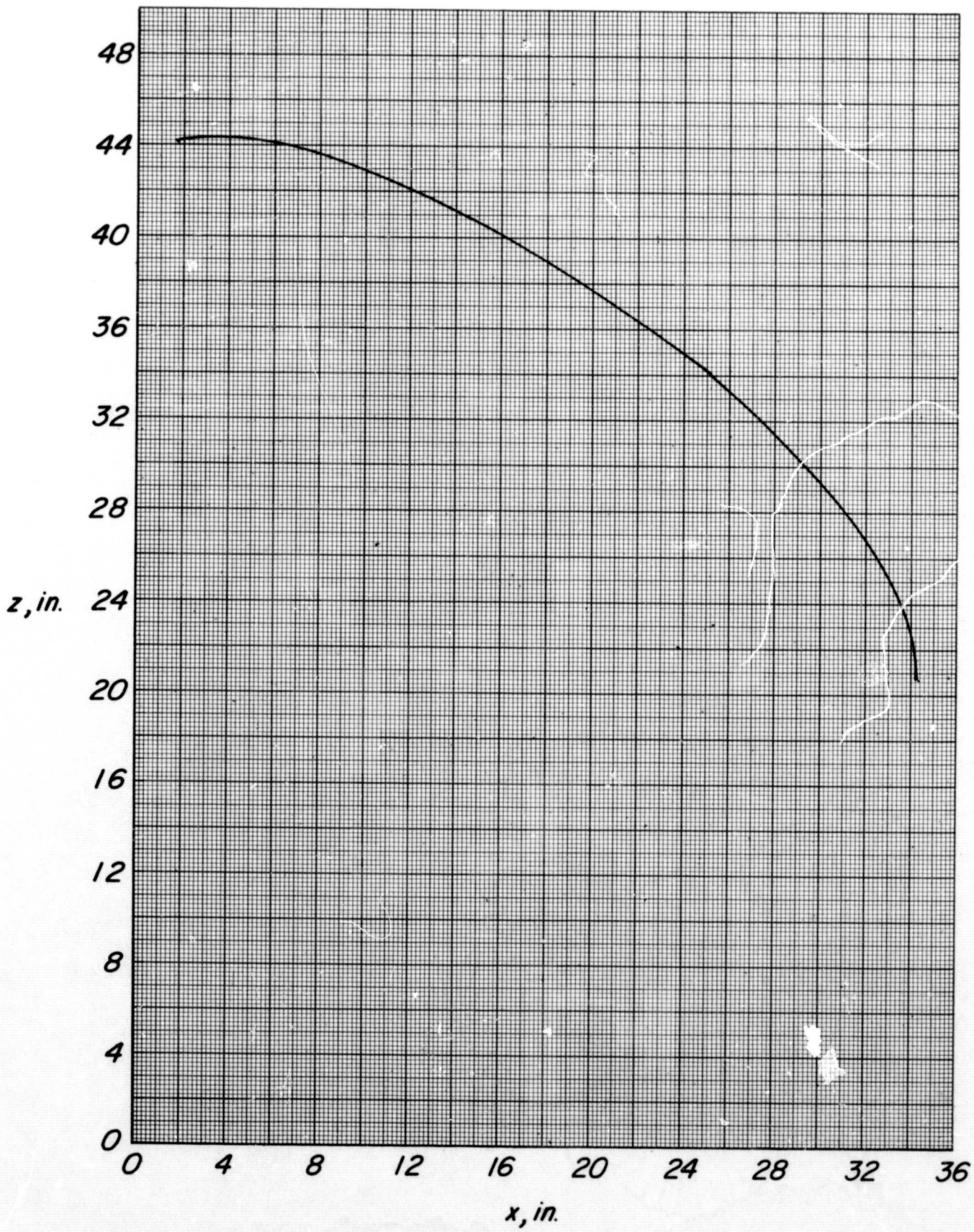

Figure 14. - Streamwise section 5.4 inches from the keel.

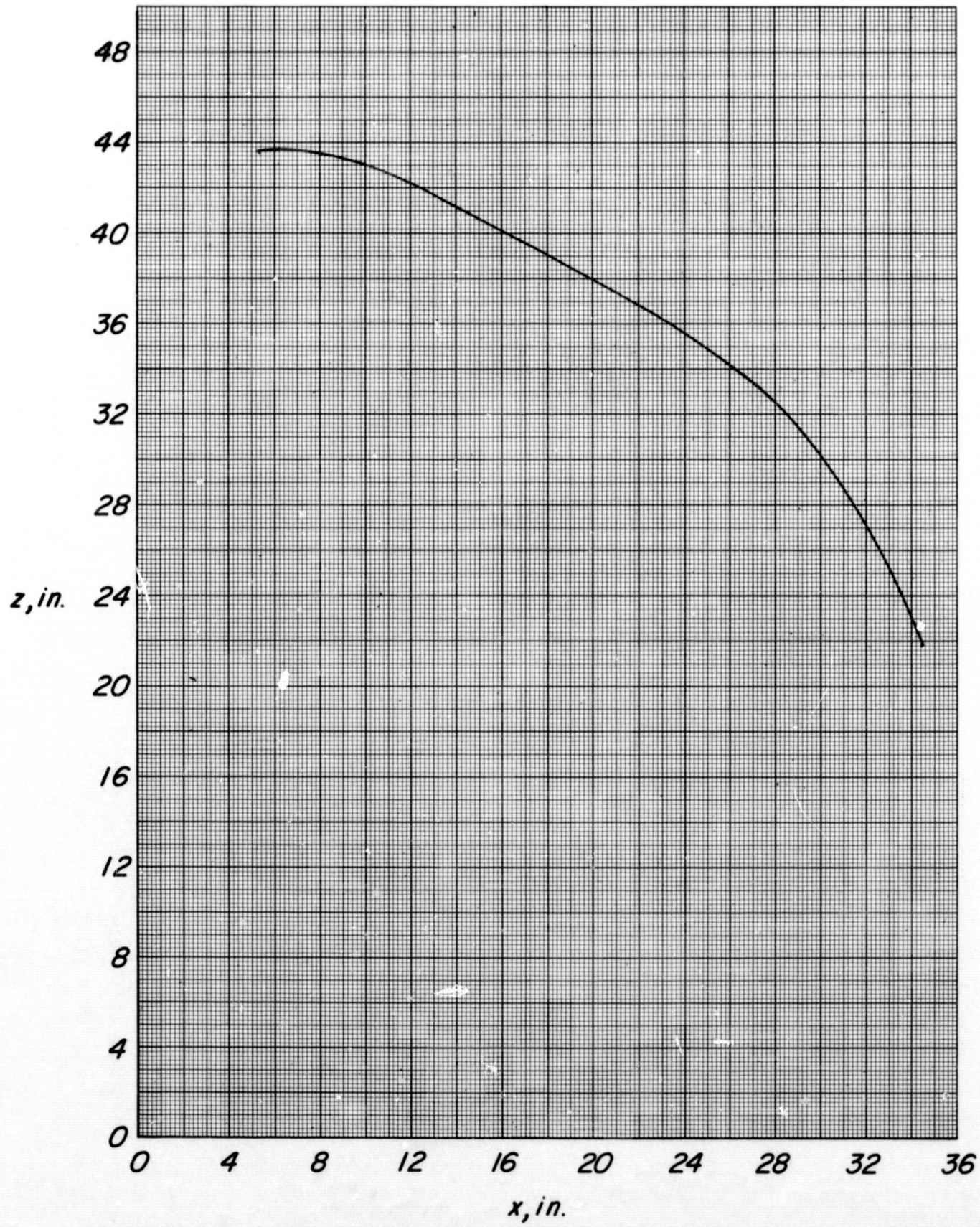

Figure 15. - Streamwise section 6.4 inches from the keel.

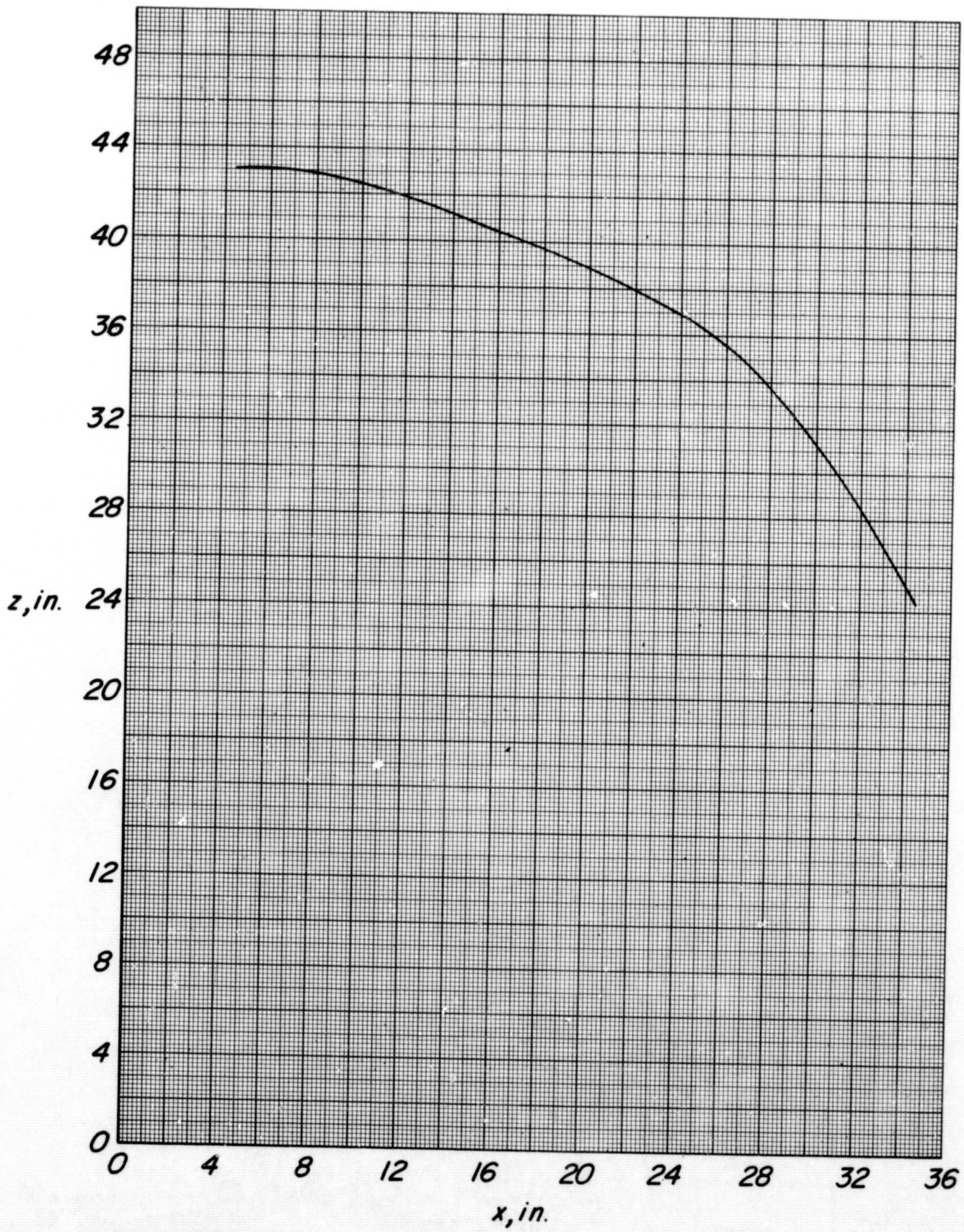

Figure 16. - Streamwise section 7.4 inches from the keel.

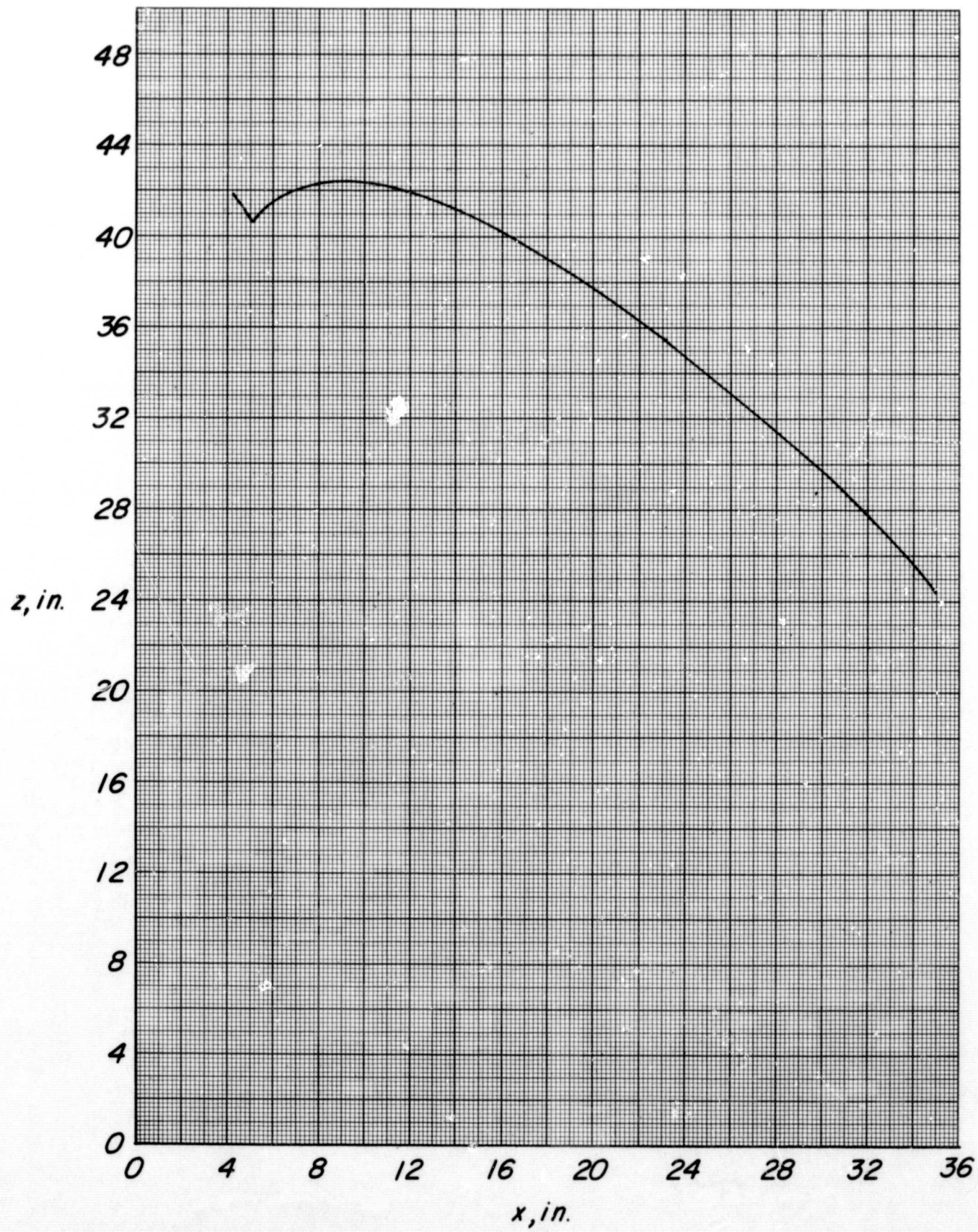

Figure 17. - Streamwise section 8.4 inches from the keel.

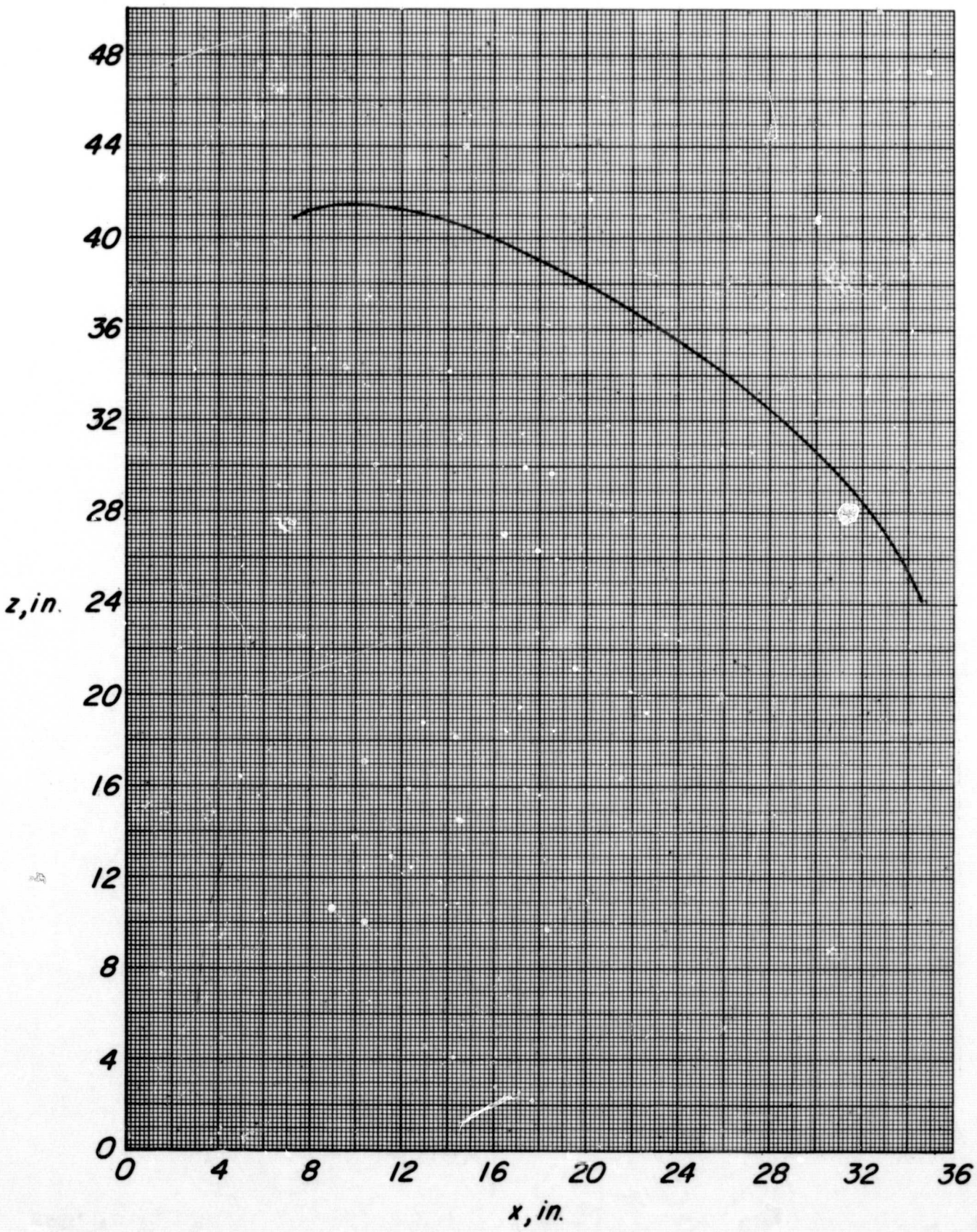

Figure 18. - Streamwise section 10.4 inches from the keel.

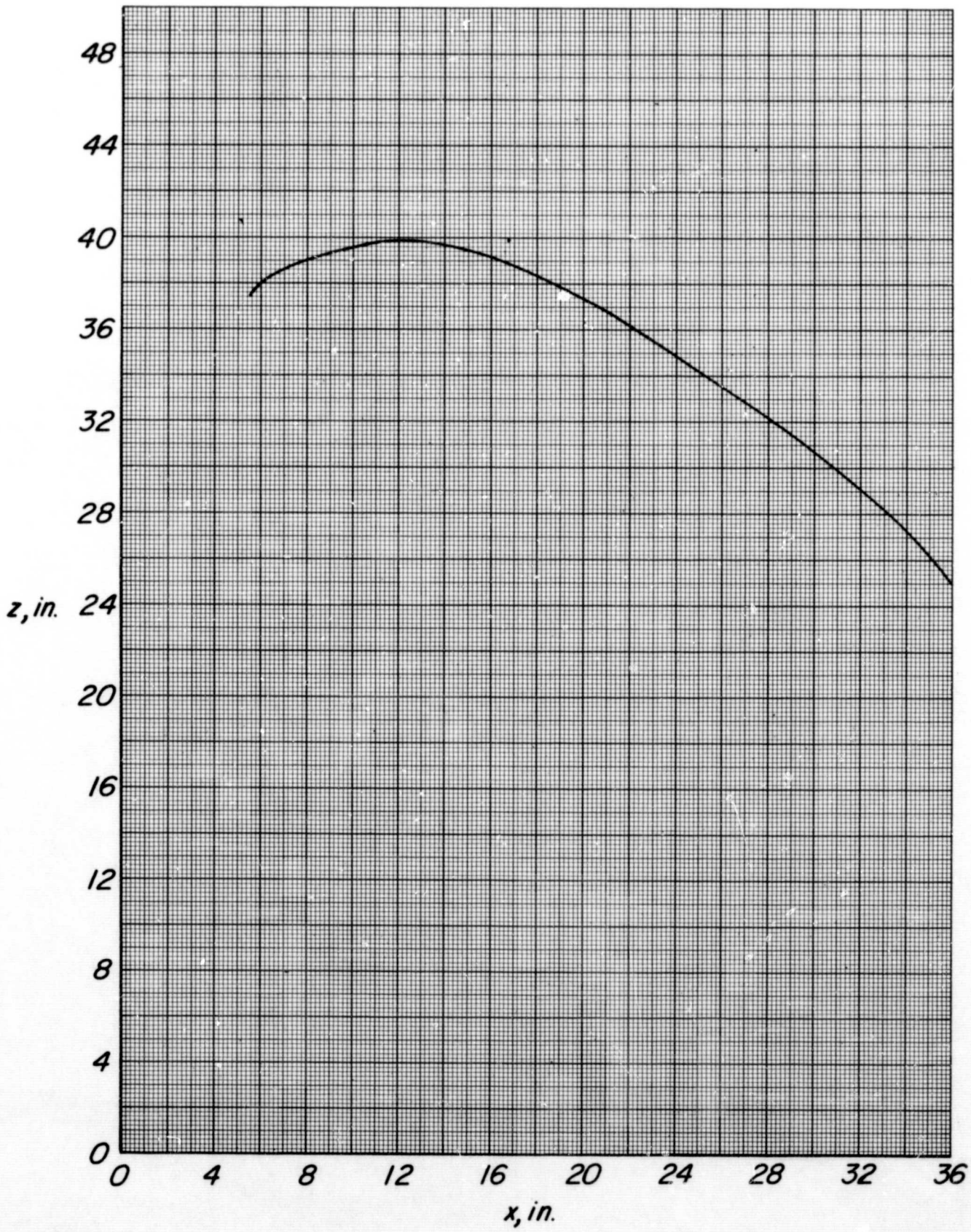

Figure 19. - Streamwise section 12.4 inches from the keel.

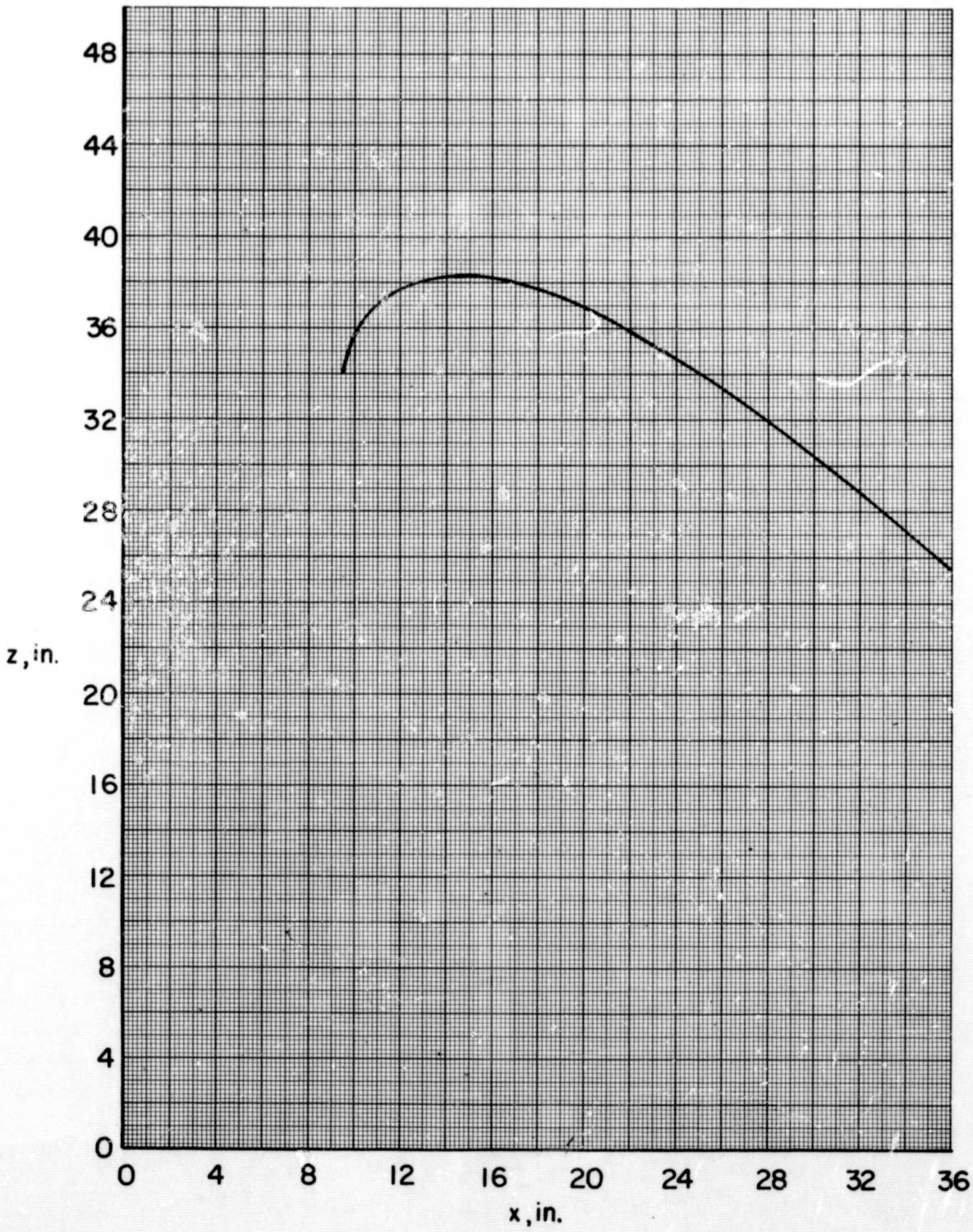

Figure 20. - Streamwise section 14.4 inches from the keel.

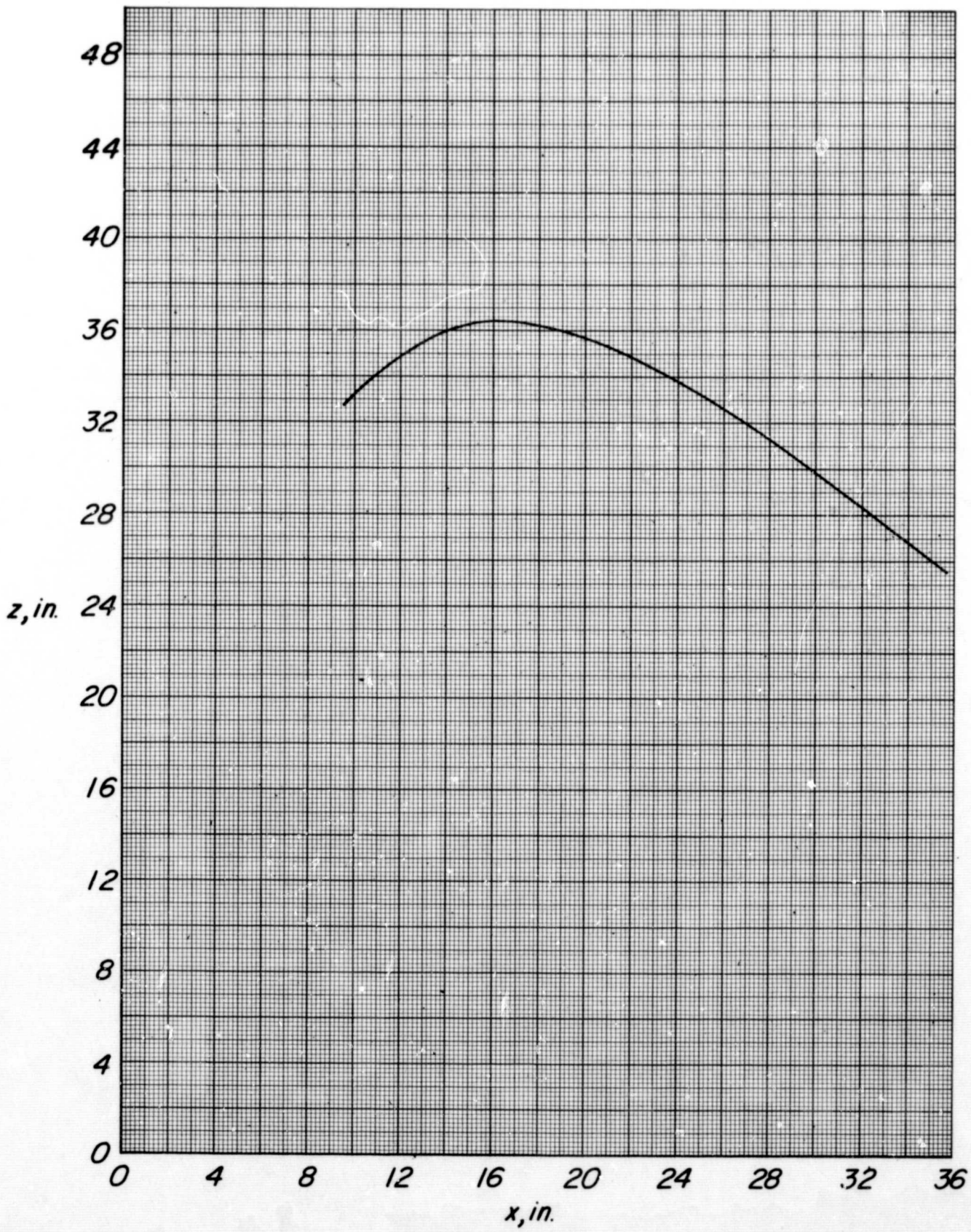

Figure 21. - Streamwise section 16.4 inches from the keel.

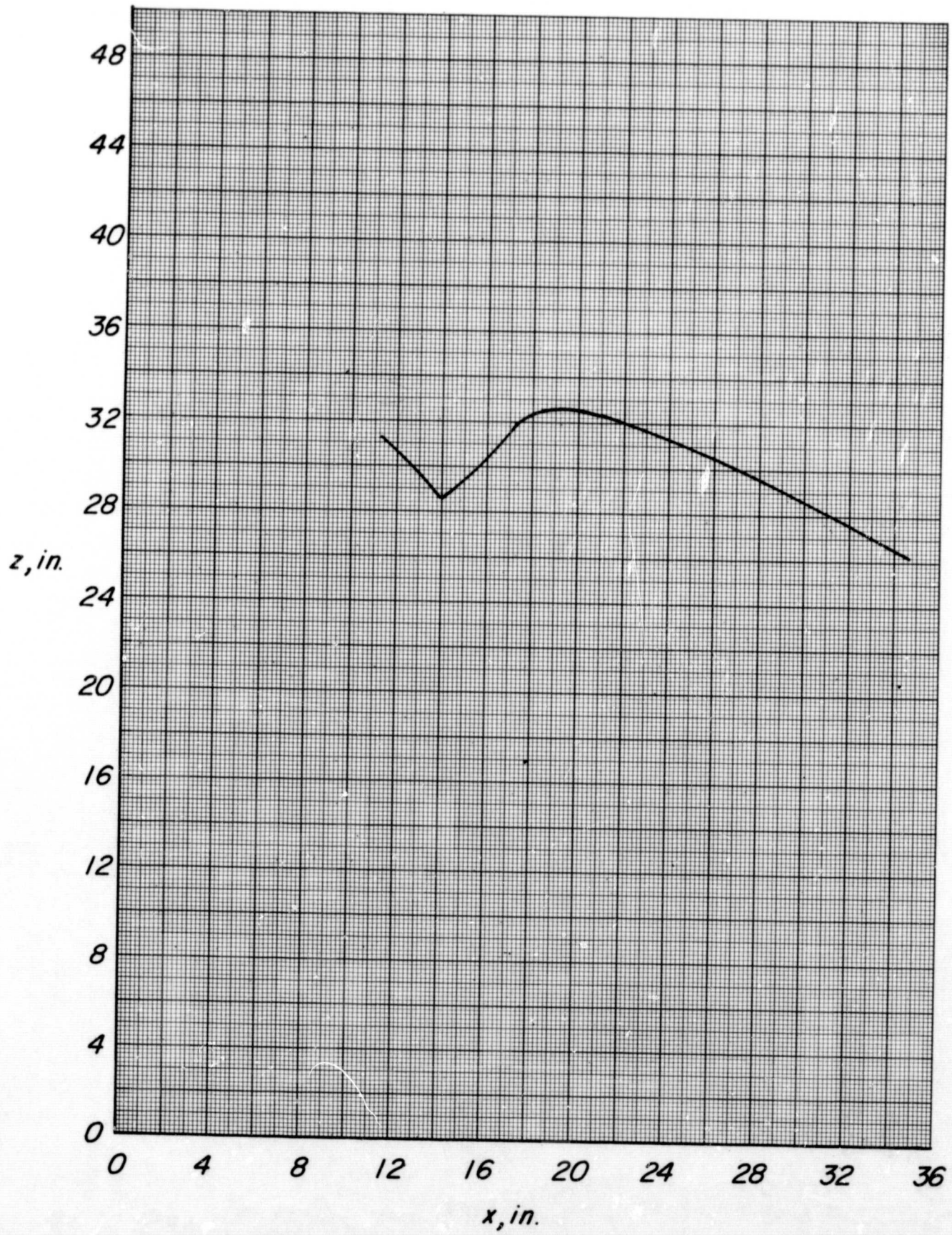

Figure 22. - Streamwise section 18.4 inches from the keel.

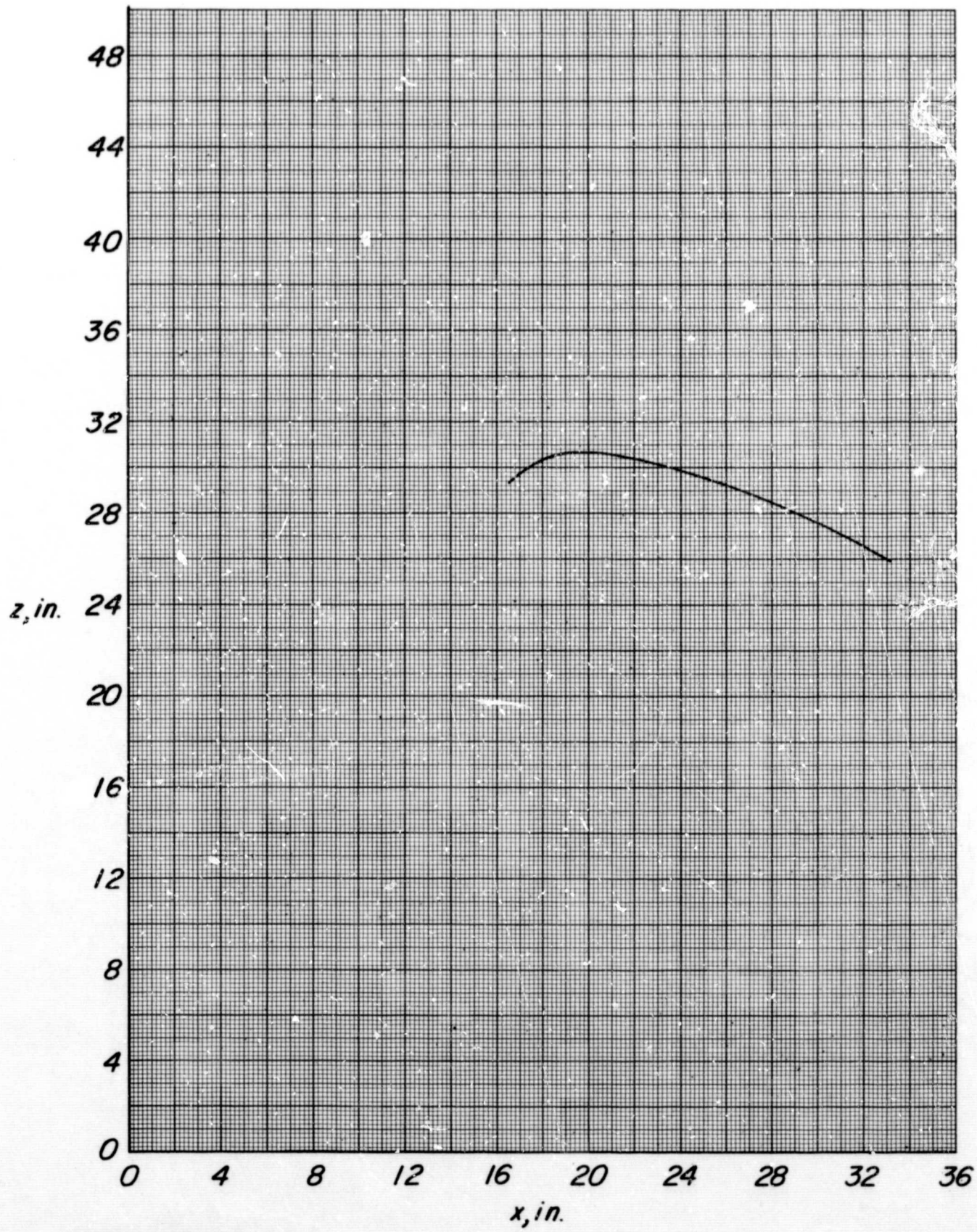

Figure 23. - Streamwise section 20.4 inches from the keel.

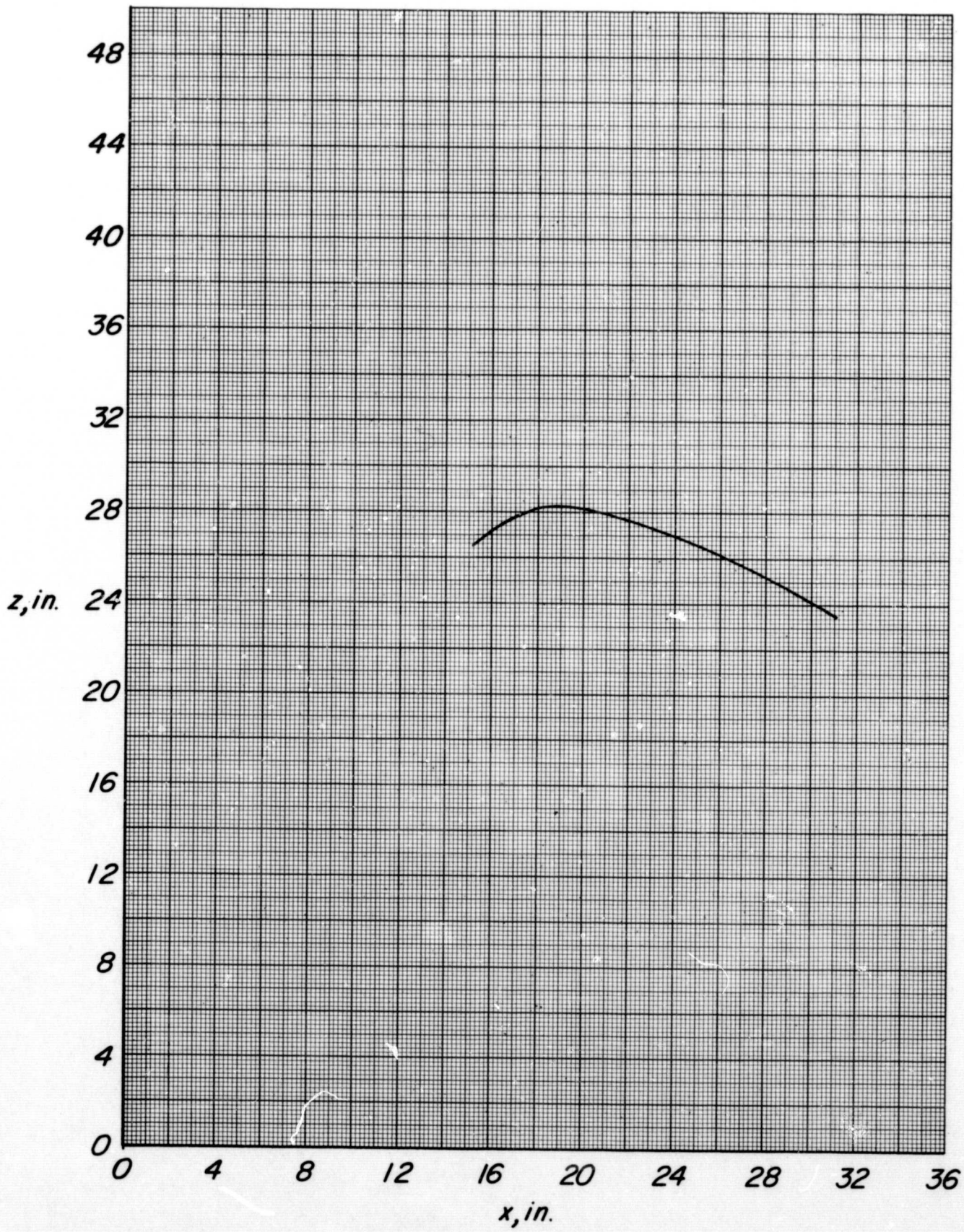

Figure 24. - Streamwise section 22.4 inches from the keel.

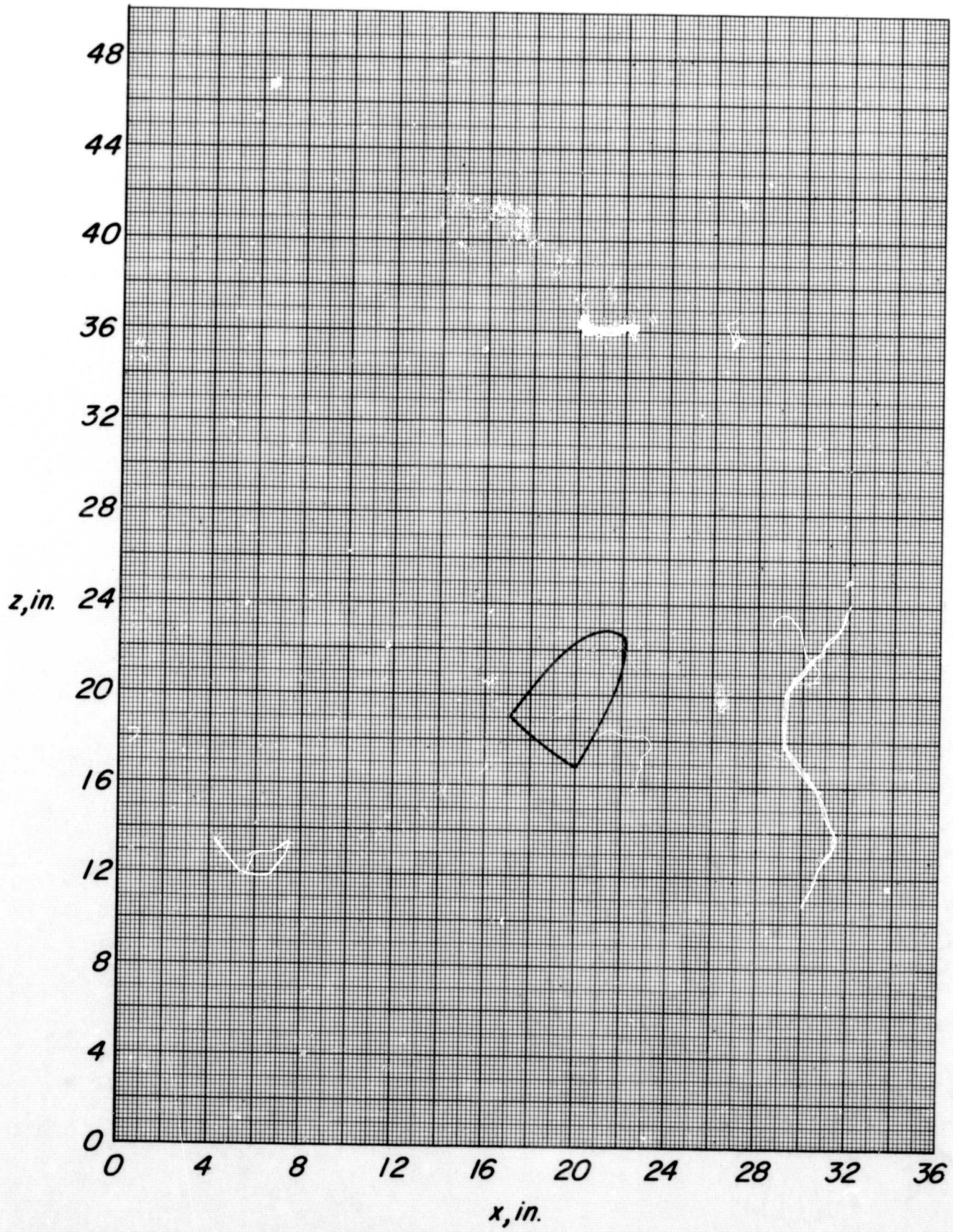

Figure 25. - Streamwise section 24.4 inches from the keel.

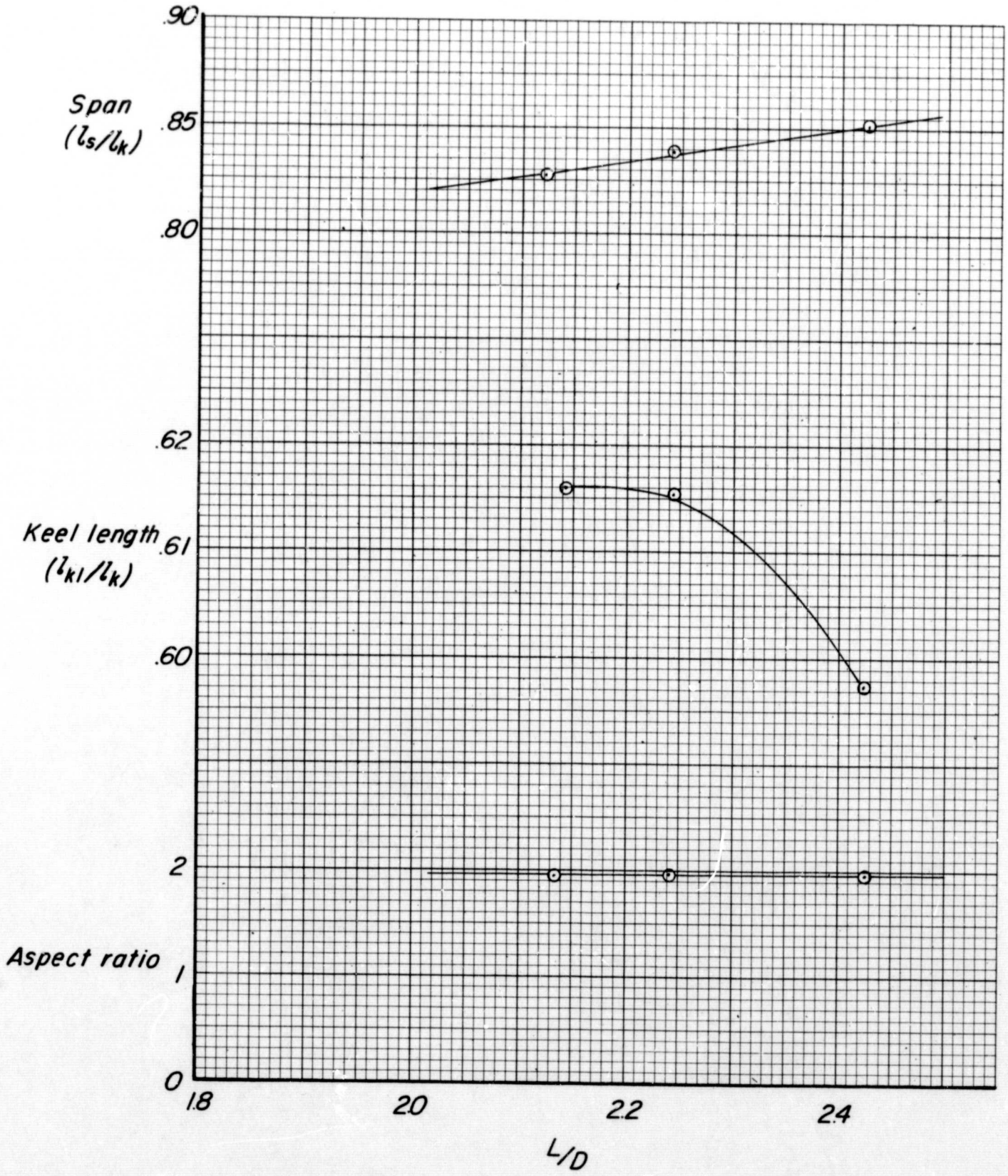

Figure 26. - Inflated keel length, inflated span, and aspect ratio versus lift-drag ratio.

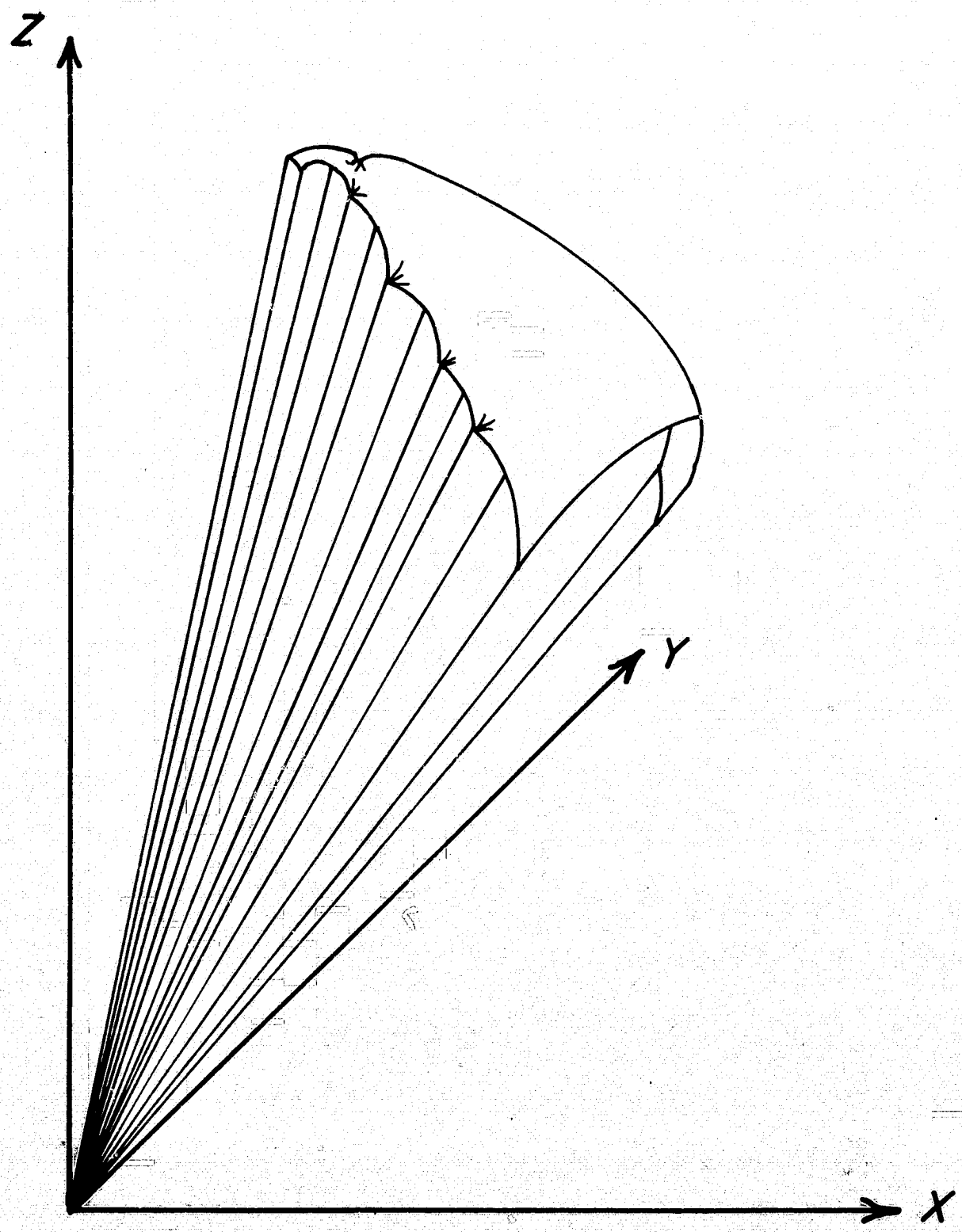

Figure 27. - Body axis system.

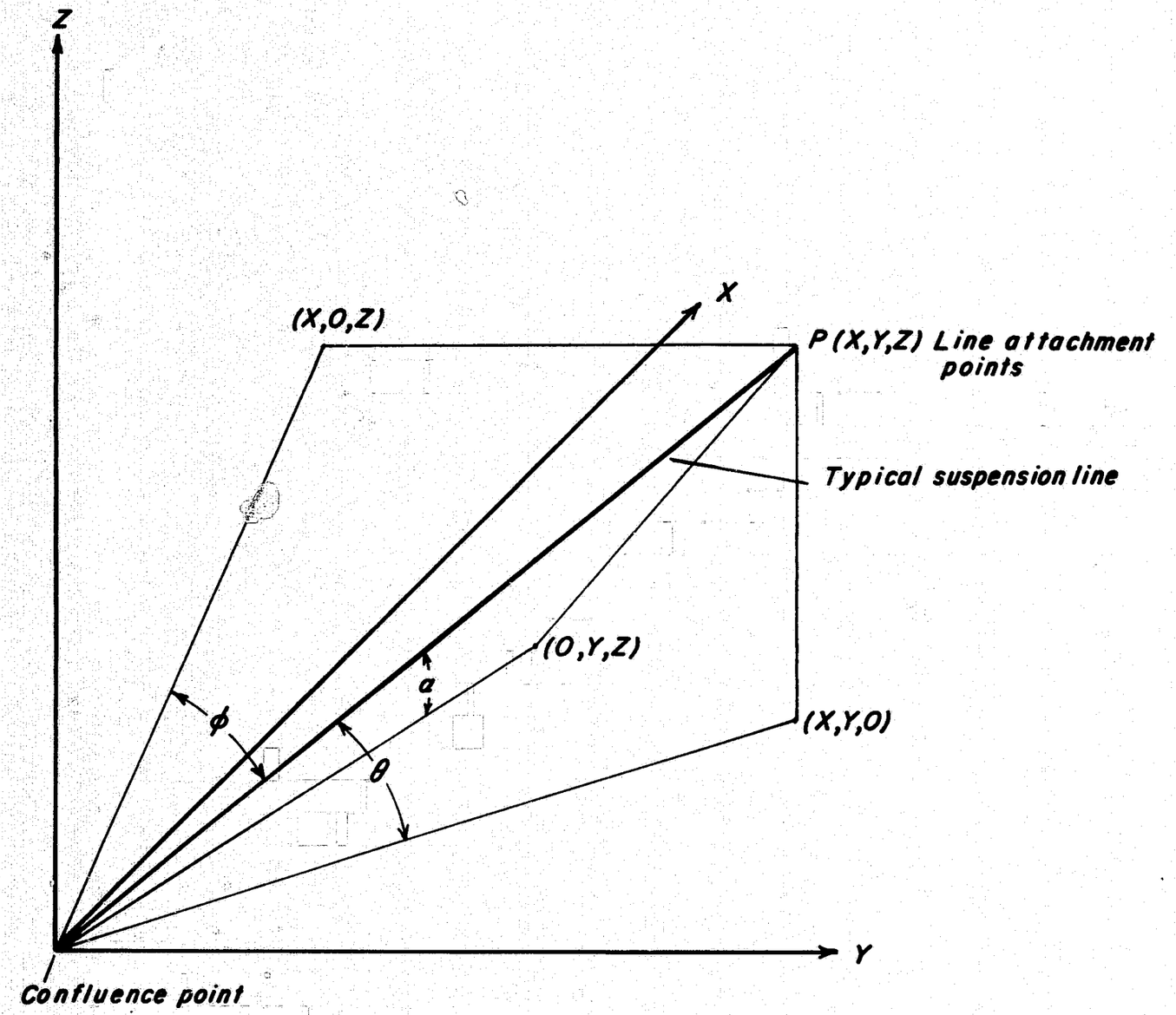

Figure 28. - Direction angles of a typical suspension line.

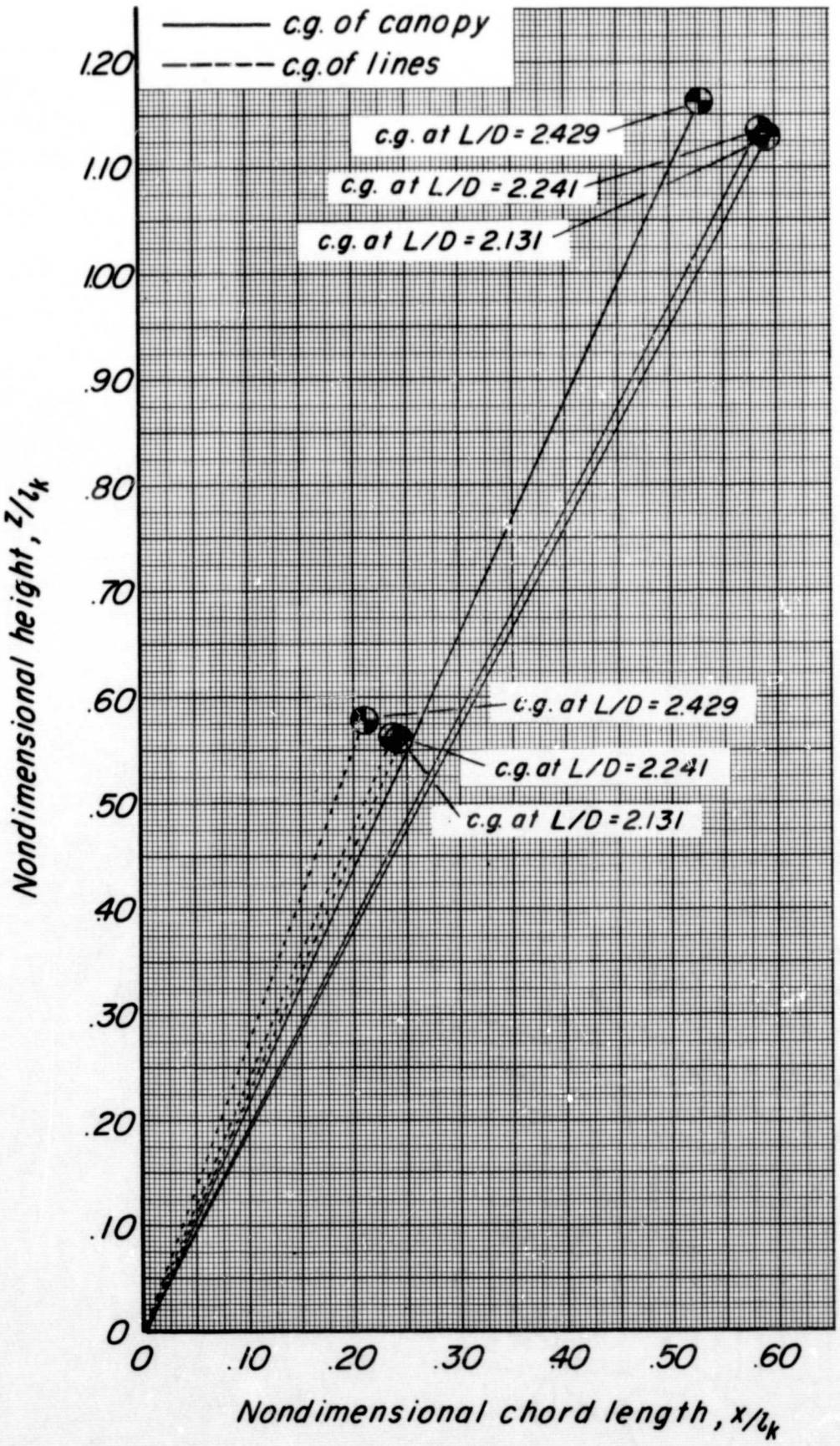

Figure 29. - Center-of-gravity shift with change in lift-drag ratio.

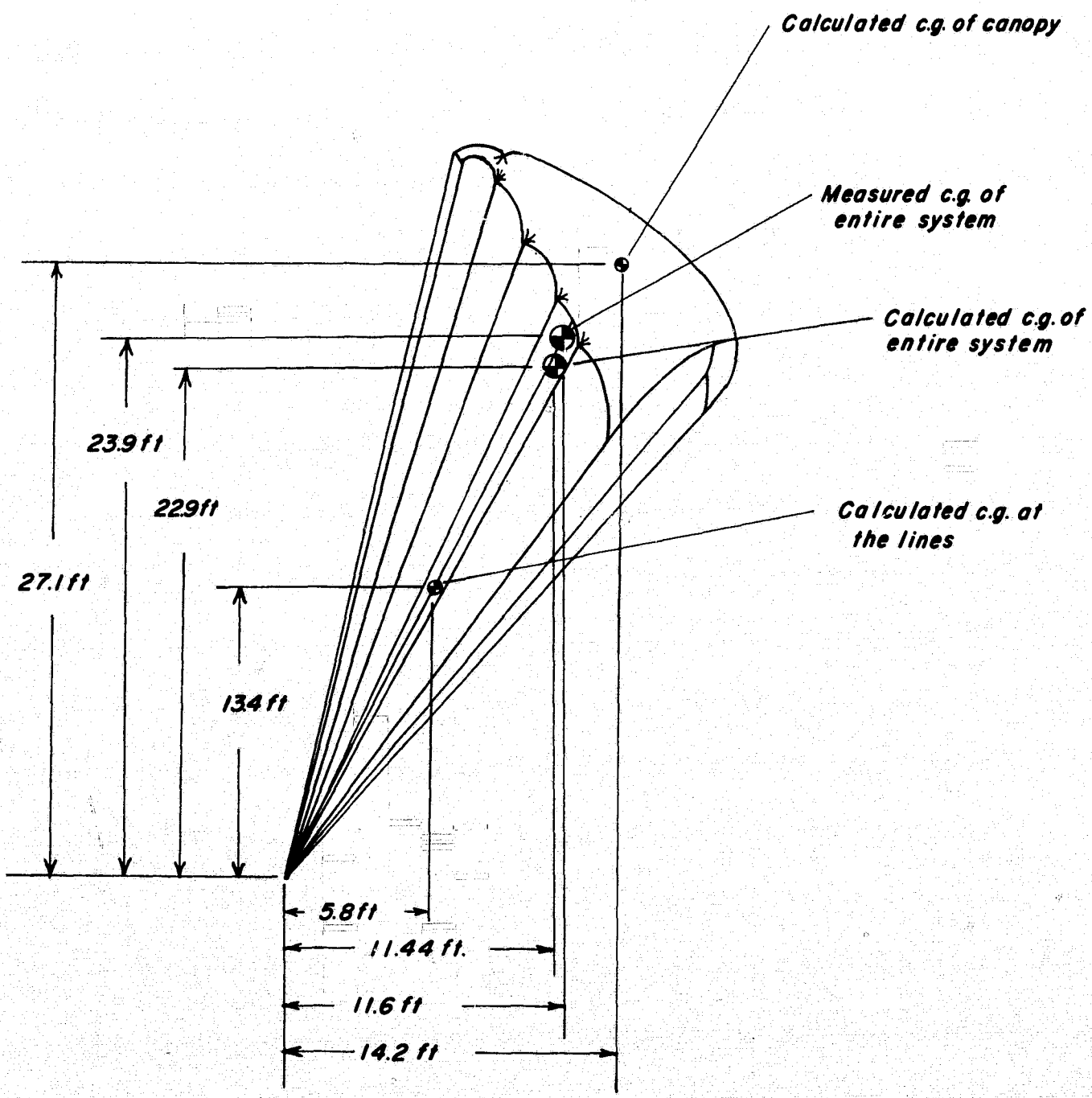

Figure 30. - Comparison of calculated and measured center-of-gravity locations of a 24-foot wing.